JOURNAL OF PETROLOGY | VOLUME 46 | NUMBER 11 | PAGES 2225–2252 | 2005 | doi:10.1093/petrology/egi053

Temporal Evolution of Magmatism in the Northern Volcanic Zone of the Andes: The Geology and Petrology of Cayambe Volcanic Complex (Ecuador)

PABLO SAMANIEGO[1,2,3]*, HERVÉ MARTIN[2], MICHEL MONZIER[3†], CLAUDE ROBIN[3], MICHEL FORNARI[4], JEAN-PHILIPPE EISSEN[3] AND JOSEPH COTTEN[5]

[1]DEPARTAMENTO DE GEOFÍSICA, ESCUELA POLITÉCNICA NACIONAL, AP. 17-01-2759, QUITO, ECUADOR

[2]UNIVERSITÉ BLAISE PASCAL, LABORATOIRE MAGMAS ET VOLCANS, UMR 6524, 5 RUE KESSLER, 63038 CLERMONT-FERRAND, FRANCE

[3]IRD, UR 031, LABORATOIRE MAGMAS ET VOLCANS, 5 RUE KESSLER, 63038 CLERMONT-FERRAND, FRANCE

[4]IRD, UMR GÉOSCIENCES AZUR, UNIVERSITÉ DE NICE-SOPHIA ANTHIPOLIS, PARC VALROSE, 06108 NICE CEDEX 2, FRANCE

[5]UMR 6538, UNIVERSITÉ DE BRETAGNE OCCIDENTALE, BP 809, 29285 BREST, FRANCE

RECEIVED JANUARY 31, 2003; ACCEPTED APRIL 15, 2005
ADVANCE ACCESS PUBLICATION JUNE 3, 2005

In the Northern Volcanic Zone of the Andes, the Cayambe Volcanic Complex consists of: (1) a basal, mostly effusive volcano, the Viejo Cayambe, whose lavas (andesites and subordinate dacites and rhyolites) are typically calc-alkaline; and (2) a younger, essentially dacitic, composite edifice, the Nevado Cayambe, characterized by lavas with adakitic signatures and explosive eruptive styles. The construction of Viejo Cayambe began >1·1 Myr ago and ended at ~1·0 Ma. The young and still active Nevado Cayambe grew after a period of quiescence of about 0·6 Myr, from ~0·4 Ma to Holocene. Its complex history is divided into at least three large construction phases (Angureal cone, Main Summit cone and Secondary Summit cone) and comprises large pyroclastic events, debris avalanches, as well as periods of dome activity. Geochemical data indicate that fractional crystallization and crustal assimilation processes have a limited role in the genesis of each suite. On the contrary, field observations, and mineralogical and geochemical data show the increasing importance of magma mixing during the evolution of the volcanic complex. The adakitic signature of Nevado Cayambe magmas is related to partial melting of a basaltic source, which could be the lower crust or the subducted slab. However, reliable geophysical and geochemical evidence indicates that the source of adakitic component is the subducted slab. Thus, the Viejo Cayambe magmas are inferred to come from a mantle wedge source metasomatized by slab-derived melts (adakites), whereas the Nevado Cayambe magmas indicate a greater involvement of adakitic melts in their petrogenesis. This temporal evolution can be related to the presence of the subducted Carnegie Ridge, modifying the geothermal gradient along the Wadati–Benioff zone and favouring slab partial melting.

KEY WORDS: *adakites; $^{40}Ar/^{39}Ar$ dating; Cayambe volcano; Ecuador; mantle metasomatism; Andes*

INTRODUCTION

The geothermal gradient along the Wadati–Benioff zone is an essential parameter that controls the nature of active margin magmatism (Martin, 1999 and references therein). Generally, a low geothermal gradient allows progressive dehydration of the subducted oceanic crust before it reaches its hydrous solidus. Liberated fluids rise through the mantle wedge, thus modifying its composition and decreasing its solidus temperature. The

*Corresponding author. Fax: +593 2 256 7847.
E-mail: Pablo.Samaniego@ird.fr
†Deceased.

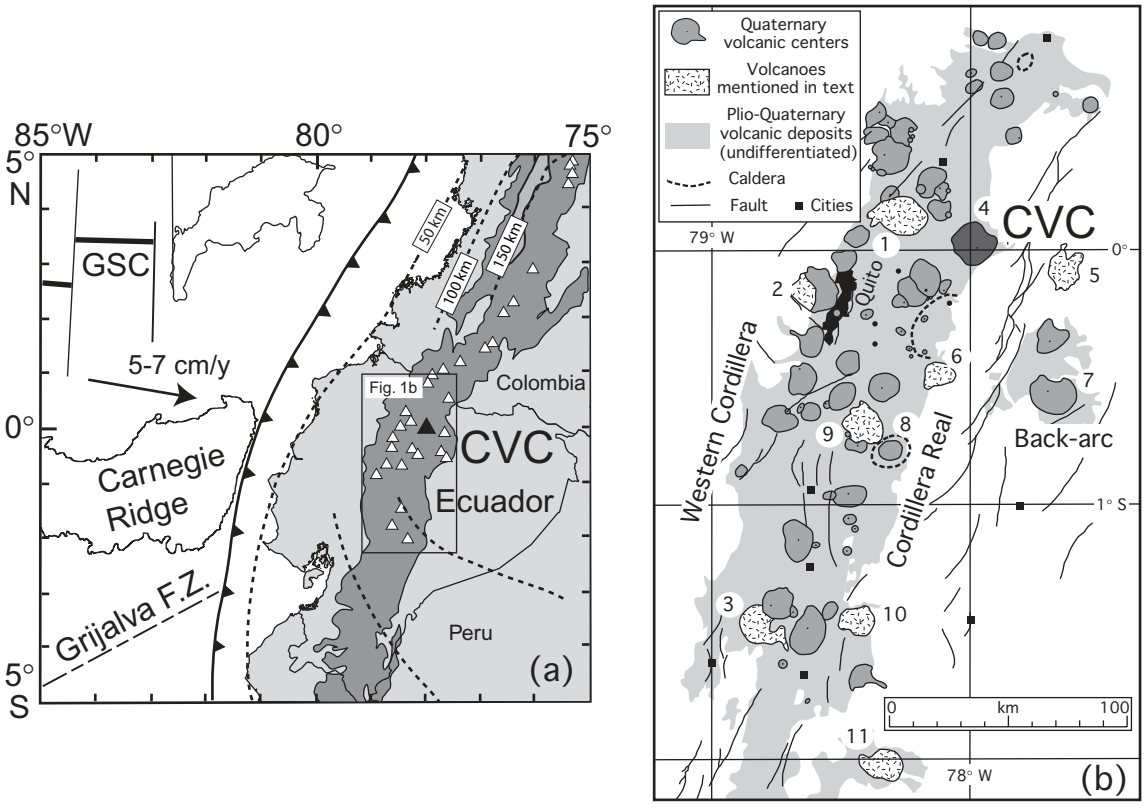

Fig. 1. (a) Geodynamic setting of the Ecuadorian arc, including the main oceanic features (modified from Gutscher *et al.*, 1999). Dotted lines correspond to the depth of the subducted slab. Andes Cordillera defined by 2000 m contour. The trench is defined by a toothed line, and active volcanoes by open triangles. Black arrow corresponds to direction of subduction. GSC, Galápagos Spreading Centre; CVC, Cayambe Volcanic Complex (represented by a black triangle). (b) Ecuadorian volcanic arc (modified from Litherland *et al.*, 1993). Names of the main edifices are: (1) Mojanda-Fuya Fuya; (2) Pichincha; (3) Chimborazo; (4) Cayambe; (5) El Reventador; (6) Antisana; (7) Sumaco; (8) Chalupas caldera; (9) Cotopaxi; (10) Tungurahua; (11) Sangay. Active faults from Egüez *et al.* (2003).

'classical' arc calc-alkaline magmatism is the final product of these processes. In contrast, when the geothermal gradient along the Wadati–Benioff zone is high, the hydrous solidus of the slab is reached before it completely dehydrates, and adakitic magmas are generated.

Slab partial melting is favoured by a young slab age (<20 Ma) whereas an old slab (>20 Ma) will be too cool to melt (Martin, 1986; Defant & Drummond, 1990; Drummond & Defant, 1990; Peacock *et al.*, 1994; Maury *et al.*, 1996; Martin, 1999; Defant *et al.*, 2001). However, adakitic magmatism may also be produced in other contexts: (1) oblique or fast subduction (Yogodzinski *et al.*, 1995); (2) initiation of subduction (Sajona *et al.*, 1993; Maury *et al.*, 1996); (3) occurrence of slab tears, favouring slab edge melting (Abratis & Wörner, 2001; Yogodzinski *et al.*, 2001); (4) existence of remnant slabs in an arc–arc collision setting (Maury *et al.*, 1996); and (5) flat slab induced by ridge subduction (Gutscher *et al.*, 2000; Beate *et al.*, 2001). It has also been proposed that melting of lower basaltic crust could produce adakites in continental arcs constructed on a thick crust (Atherton & Petford, 1993).

In Ecuador, the Northern Volcanic Zone of the Andes (NVZ) results from the subduction of the 12–20 Ma Nazca Plate beneath the South American Plate. On the basis of seismic and gravimetric data, the crustal thickness in this region has been estimated to be >50 km (Feininger & Seguin, 1983; Prévot *et al.*, 1996; Guillier *et al.*, 2001). Moreover, the main part of NVZ developed facing the Carnegie Ridge, which corresponds to the trace of the Galápagos hotspot across the Nazca Plate (Fig. 1a). Subduction of the ridge has been continuing since at least 6–8 Ma (Gutscher *et al.*, 1999), implying its presence below the volcanic arc at the present day. However, the subducted slab beneath the Ecuadorian arc is characterized by weak seismicity, making the definition of the slab geometry difficult (e.g. Pennington, 1981; Gutscher *et al.*, 1999). More recently, Guillier *et al.* (2001) concluded that between 0° and 1°S, the slab plunges continuously and reaches 100 km depth beneath the volcanic front. Unfortunately, they could not determine the depth of the subducted slab further eastward.

The coexistence of 'classical' calc-alkaline and 'adakitic' lavas in the Ecuadorian arc has been demonstrated by

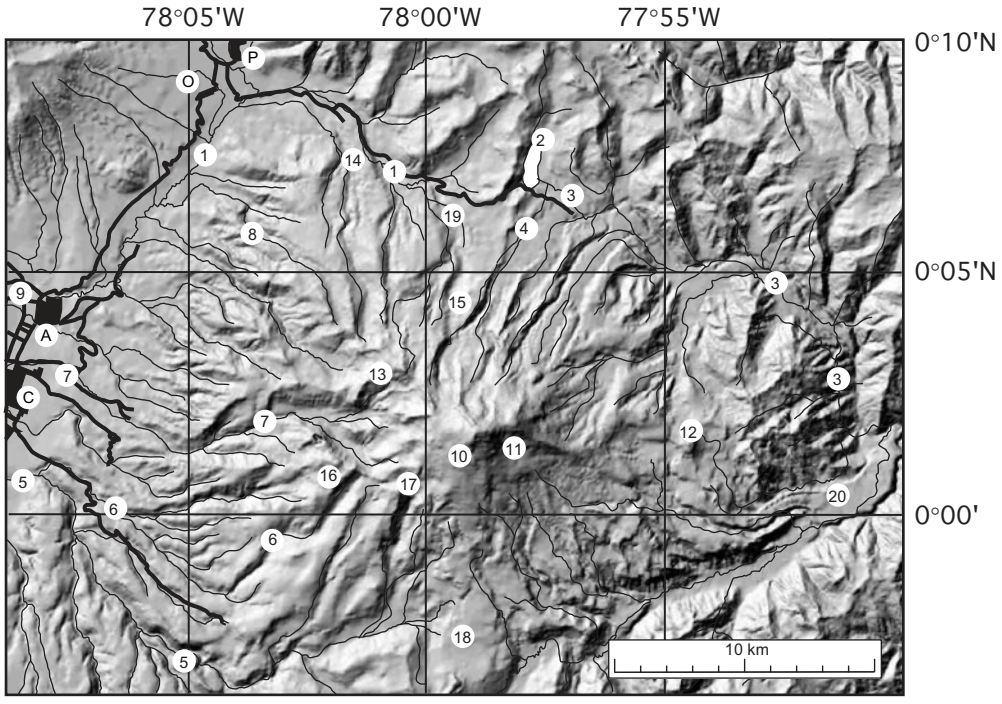

Fig. 2. Shaded relief image (illuminated from the NW), representing the Digital Elevation Model (DEM) of the Cayambe volcanic complex. Digital information, provided by M. Souris (IRD), was generated from 1:50 000 topographic maps of the Instituto Geográfico Militar, Quito. The geographical localities referenced in text are shown. Heavy lines represent main roads. C, Cayambe; A, Ayora; O, Olmedo; P, Pesillo. 1, Río (river) La Chimba; 2, San Marcos lake; 3, Río Azuela; 4, Río San Pedro; 5, Río Guachalá; 6, Río Monjas; 7, Río Blanco; 8, Río Pulisa; 9, Río Granobles; 10, Nevado Cayambe Main Summit; 11, Nevado Cayambe Secondary Summit; 12, Cono La Virgen; 13, Angureal peak; 14, Hierba Buena; 15, Las Antenas; 16, Pucará; 17, Mountain Refuge; 18, La Dormida; 19, La Chimba; 20, Planada de La Virgen.

several workers (Monzier *et al.*, 1997; Samaniego, 2001; Bourdon *et al.*, 2002*a*, 2003). In addition, large edifices, such as Cayambe (Samaniego *et al.*, 2002), Pichincha (Bourdon *et al.*, 2002*a*) and Mojanda-Fuya Fuya (Robin *et al.*, 1997, in preparation), illustrate an evolution from an old calc-alkaline edifice to young, adakitic magmatism. The aim of this study is: (1) to describe and discuss the temporal magmatic transition in a single edifice; (2) to propose and to test petrogenetic hypotheses that account for the compositional evolution; (3) to establish the relationships between petrogenesis and geodynamics, in order to constrain adakite genesis in the Northern Andes.

LOCATION AND STRUCTURE OF THE CAYAMBE VOLCANIC COMPLEX

In Ecuador, volcanoes of the NVZ are distributed in three alignments: the volcanic front in the Western Cordillera, the main arc in the Eastern Cordillera (Cordillera Real), and the back-arc region in the Eastern foothills (Fig. 1). In the northern part of the Eastern Cordillera, the construction of the Cayambe Volcanic Complex (CVC) has been controlled by regional faults, oriented N35°E, the largest of which is the 'La Sofía–Río Chingual' fault (Tibaldi & Ferrari, 1992; Ego *et al.*, 1996) (Fig. 1b). The upper crust beneath the volcano mainly consists of Triassic semi-pelitic schists, paragneisses and granites of the Loja Division (Litherland *et al.*, 1993). The lower crust in the Ecuadorian arc is largely unknown, as outcrops and xenoliths are lacking. On the basis of xenoliths hosted in late Cenozoic volcanic deposits of southwestern Colombia, Weber *et al.* (2002) suggested that lower crust in this part of NVZ is basaltic in composition, and that it is transformed into amphibolite- or granulite-facies rocks.

The CVC has a rectangular shape (24 km E–W and 18 km N–S, Fig. 2); its base is about 3000 m in elevation on the western side, and 3400–3800 m on the eastern side. The upper part of the complex is elongated WSW–ENE, with two western and eastern summits, only 1·5 km apart, which culminate at 5790 and 5487 m. Above 4900 m, an enormous glacial cap, at least 30–50 m thick, covers the upper part of the complex. From this ice cap, glaciers extend down the slope to 4200–4400 m on the wet, eastern Amazonian side, but only to 4600–4800 m on the drier, western side.

The western side of CVC displays regular gentle slopes (5–10°), carved by U-shaped, radially oriented glacial

valleys, contrasting with the other sides, which show an uneven topography and dip slopes (Fig. 2). Such a morphological contrast is related to different lithologies, eruptive dynamics, and ages: the western side is mainly made of old thick lava flows, whereas the eastern side mainly consists of younger lava flows and domes. As the domes exposed on the northern side have been active in recent times, the upper part of this flank is abrupt, and differs from the gentle and regular southern side. Moreover, the upper western part of the complex exposes a horseshoe-shaped structure open to the west. Several high points define this structure, the main one being the Angureal peak (4815 m). This structure results from a large collapse event that has affected volcanic units of different ages: the southern wall consists of lava flows from the old edifice, whereas the lavas to the north of the Río Blanco valley are more recent.

The CVC comprises two main volcanoes (Figs 2 and 3): (1) a basal, mostly effusive, stratovolcano, largely dissected by erosion and called the 'Viejo Cayambe' (VCAY); (2) a younger, more explosive, composite edifice, the 'Nevado Cayambe' (NCAY), constructed over the central and eastern ruins of VCAY. The NCAY volcano consists of three edifices: the Angureal cone (NCAY-ANG), the Main Summit edifice (NCAY-MS), and the more recent Secondary Summit (NCAY-SS), developed on the eastern side of the main summit. On the eastern flank, a satellite vent, named 'Cono La Virgen' (CLV), has developed during the Late Holocene.

ERUPTIVE CHRONOLOGY

Sample preparation and $^{40}Ar/^{39}Ar$ dating method

Six lavas have been dated by the $^{40}Ar/^{39}Ar$ method on whole-rock bulk samples. Thin slabs (350 μm) were cut and fragments without phenocrysts were hand picked under a binocular microscope. Weights of between 160 and 260 mg of rock were wrapped in copper-foil packets and irradiated for 1 h with cadmium shielding in the 5C position at the nuclear reactor of McMaster University (Hamilton, Canada). The samples were associated with the Fish Canyon sanidine (FCS) as a neutron flux monitor of the reactor (J-value determination) assuming an FCS age of 28·02 Ma (Renne *et al.*, 1998).

Age determinations (Table 1) were performed in the Laboratory of Geochronology of UMR Géosciences Azur at the University of Nice, France. Step-heating was performed in a double-vacuum, high-frequency heated furnace, and the samples were analysed with a mass spectrometer composed of a 120° M.A.S.S.E tube, a Bauer-Signer GS98 source, and a Balzers electron multiplier. Heating lasted 20 min for each temperature step, followed by 5 min for clean-up of the released gas, before introducing the gas into the spectrometer. Argon isotopes were of the order of 100–2000, 100–1000 and 2–200 times the blank levels for masses 40, 39 and 36, respectively. In some high-temperature steps, the measured ^{36}Ar was near the blank level. Mass discrimination was monitored by regularly analysing air pipette volume.

The criteria generally used in the laboratory for defining a 'plateau' age are the following: (1) it should contain at least 70% of total ^{39}Ar released; (2) there should be at least three successive step-heating fractions in the plateau; and (3) the integrated age of the plateau (weighted average of apparent ages of individual fractions comprising the plateau) should agree with each apparent age of the plateau within a 2 sigma (2σ) error. In this study, only two samples provided plateaux with more than 70% of total ^{39}Ar released; therefore, we consider also smaller plateaux including only 48–57% of total ^{39}Ar released.

Ages were calculated from measured isotope ratios corrected for mass discrimination, system blanks and interfering isotopes produced during irradiation. The error on the $^{40}Ar^*/^{39}Ar_K$ ratio of the monitor is included in the plateau age error bar calculation. Ratios of Ca/K, determined from the measurement of argon isotopes produced during irradiation from these elements, are used in the identification of minerals that may have contributed argon in each step-heating fraction.

Isochron ages were calculated using a reverse isochron diagram, plotting $^{36}Ar/^{40}Ar$ versus $^{39}Ar/^{40}Ar$, using the least-squares method (York, 1969). This provides a check on the initial $^{40}Ar/^{36}Ar$ ratio, which is generally near atmospheric values.

Main volcanic units

Basal volcano or 'Viejo Cayambe' (VCAY)

The oldest volcanic units chiefly form the western part of the complex. The radial distribution of shallow-dipping lava flows shows that the first volcanic centre was located near the central part of the complex, at an altitude of about 4300–4400 m. Assuming a 16–18 km width and 1400–1600 m high cone, the estimated volume of the VCAY edifice is 100–130 km^3.

Older deposits consist of two-pyroxene andesitic lava flows (57–61 wt % SiO_2, normalized to an anhydrous basis) and scarce interlayered breccias. In the Río Blanco valley, these deposits are 400–500 m thick (VCAY1, Fig. 3). On the lower western slope of the complex (e.g. Río Pulisa), the lava pile overlies andesitic breccias. Conversely, on the southwestern flank of the volcano (Río Monjas and Río Guachalá valleys), a 200 m thick series of two-pyroxene dacitic lava flows (67–68 wt % SiO_2) and a 40–50 m thick sequence of reworked rhyolitic pumice deposits (72–73 wt % SiO_2) indicate periods of siliceous and explosive activity during the late stages of VCAY

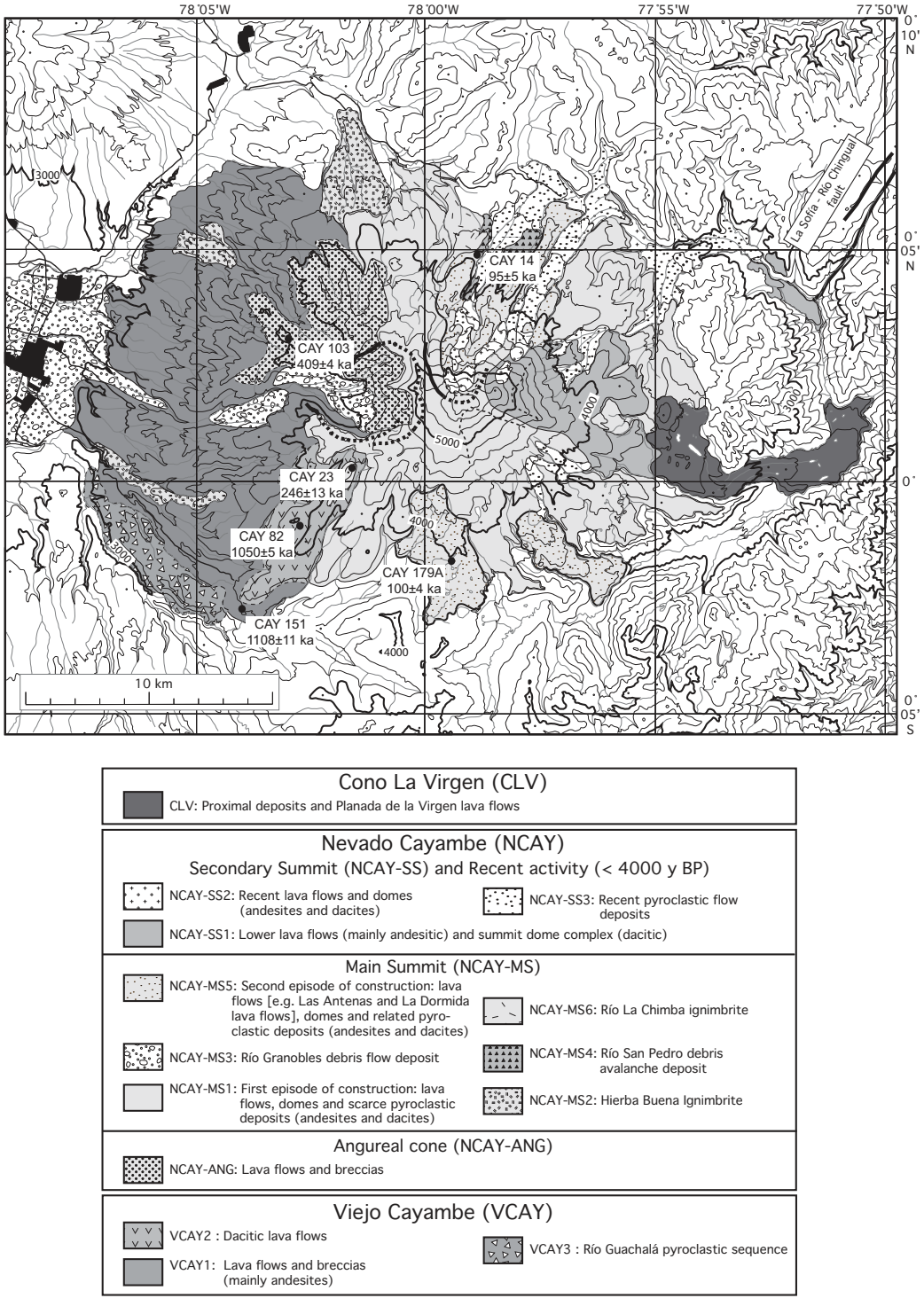

Fig. 3. Simplified geological map of the Cayambe volcanic complex. Bold curves represent collapse rims, in some cases buried (dotted curves). Contour interval is 200 m. New $^{40}Ar/^{39}Ar$ age dates are indicated (see also Table 1).

(units VCAY2 and 3, Fig. 3). These deposits, together with the arc-shaped southern wall of the Río Blanco valley, reveal that the evolution of the VCAY edifice ended in a large caldera-forming eruption.

Two $^{40}Ar/^{39}Ar$ ages have been obtained on VCAY rocks (Table 1; Fig. 3). A lower andesitic lava flow (VCAY1 unit) yielded a plateau age of 1108 ± 11 ka, and a dacitic lava flow from VCAY2 unit gave a plateau

Table 1: $^{40}Ar/^{39}Ar$ ages for rocks from Cayambe volcanic complex

Sample number	Volcanic unit & rock type	Map (Fig. 3) label	SiO_2 (wt %)	UTM coordinate*		Weight (mg)	Lab number	Prefered 'plateau' age			Inverse correlation diagram		
				Easting	Northing			Age ± 2σ	^{39}Ar %†	Steps‡	Isochron age	Ri§	MSWD¶
CAY151	Basal lava flow	VCAY1	60·19	08264	99949	230·5	M1732	1108 ± 11	48	8–12/16	1159 ± 56	285·5 ± 5·6	60·0
CAY82	Dacitic lava flow	VCAY2	66·89	08287	99984	210·9	M1721	1050 ± 5	56	9–11/16	1069 ± 16	294 ± 2·5	18·5
CAY103	Angureal lava flow	NCAY-ANG	63·63	08284	99056	260·3	M1731	409 ± 4	56	9–12/16	418 ± 10	295·8 ± 2·7	19·3
CAY23	'Refuge' lava flow	NCAY-MS1	63·60	08312	00007	197·2	M1723	246 ± 13	57	7–13/17	247 ± 22	295·2 ± 1·3	10·5
CAY179A	'La Dormida' lava flow	NCAY-MS5	65·40	08348	99972	219·1	M1733	100 ± 4	74	10–13/19	92 ± 12	298·5 ± 2	18·0
CAY14	'Las Antenas' lava flow	NCAY-MS5	63·62	08360	00085	164·8	M1753	95 ± 5	84	6–9/19	94 ± 4	294·1 ± 1·2	0·8

*Locations are given to 100 m using the UTM metric grid (1956, Provisional South America, zone 17), which is shown on Instituto Geográfico Militar maps.
†Percentage of total ^{39}Ar included in the plateau age.
‡Number of temperature steps included in the plateau versus total number of steps.
§($^{40}Ar/^{36}Ar$) initial ratio.
¶Mean square of weighted deviates.

age of 1050 ± 5 ka. Thus, the development of the VCAY edifice lasted at least 100 kyr, between >1·1 Ma and *c.* 1·0 Ma.

The Angureal cone or intermediate edifice

Relics of the Angureal cone (NCAY-ANG, Fig. 3) overlie the remnants of VCAY. They are represented by thick lava flows and subordinate monolithologic breccias in the upper valley of Río Blanco, and form the volcanic pile of Angureal peak. Steep dips show that the vent of NCAY-ANG was located 2 km east of the VCAY centre (i.e. ∼3 km west of the actual main summit), at about 5200 m elevation. This edifice was affected by the subsequent sector collapse, related to the horseshoe-shaped scar of the upper Río Blanco valley (Figs 2 and 3). The NCAY-ANG lavas consist of amphibole ± biotite-bearing dacites (64–68 wt % SiO_2), which clearly differ from the VCAY two-pyroxene dacites. All the rocks are characterized by hydrothermal alteration (including the presence of sulphur minerals). The $^{40}Ar/^{39}Ar$ whole-rock age for a lower lava from this edifice is given by a plateau age of 409 ± 4 ka (Fig. 3). Thus, the volcanic activity resumed after a period of quiescence of *c.* 600 000 years, which is marked by an important erosive discordance.

The Nevado Cayambe Main Summit

To the east of the Angureal cone, the most voluminous stratovolcano of the CVC (∼130–170 km^3) forms the main summit (NCAY-MS). This part of the volcano has had a complex development and experienced various eruptive styles during at least two construction stages.

First episode of construction (NCAY-MS1). The present main summit was constructed by a series of andesitic and dacitic (61–67 wt % SiO_2) lava flows and domes, which are well represented on the southern flank, around Refuge and Pucará peaks (Figs 2 and 3). The mineral assemblage in these lavas is typical of NCAY rocks: Pl + Amph + Cpx + Opx + Mag (abbreviations after Kretz, 1983). During this period, on the northwest flank, at the foot of Angureal peak, block-and-ash deposits were emplaced within a paleo-valley, suggesting that a summit dome complex may have existed on this flank. Dating of a dacite from the Refuge area yields a plateau age of 246 ± 13 ka (Table 1; Fig. 3).

The Hierba Buena ignimbrite (NCAY-MS2). Large outcrops of a 150–200 m thick welded ignimbrite sheet have been found in the northwestern part of the complex. The deposit shows prismatic jointing and bears decimetric glassy blocks, is dacitic in composition (66–67 wt % SiO_2), and is characterized by the mineral assemblage Pl + Amph + Cpx + Opx + Mag. On the basis of petrological and stratigraphic evidence, other welded or indurated ignimbrite deposits preserved in the Río Monjas and Río Pulisa valleys are believed to have formed during

the same pyroclastic event. The Hierba Buena ignimbrite represents an important explosive event, which probably occurred during (or just after) the first stage of NCAY construction (Fig. 3).

Debris avalanche deposits (NCAY-MS3, 4). Two debris avalanche deposits have been recognized. A 10–20 m thick chaotic deposit, consisting of a clay-rich matrix and blocks with typical jigsaw fractures, has been observed in the Río Granobles and Río Guachalá valleys (NCAY-MS3, Fig. 3). The blocks are two-pyroxene andesites, amphibole-rich andesites and dacites, often with hydrothermal alteration. This deposit spread out over the Cayambe plain, strongly suggesting a relationship with the Río Blanco collapse event. Given that the collapse affected the block-and-ash deposits at the eastern foot of Angureal peak, we propose that the sector collapse occurred at the end of the first construction stage of NCAY, and we estimate an age of <200 ka for this event.

A less voluminous and apparently less heterogeneous (amphibole-bearing andesites, 61–63 wt % SiO_2) debris avalanche deposit was channelled by the Río San Pedro valley on the northern flank of the complex (NCAY-MS4, Fig. 3). Downward, this deposit turns into a sequence of lahars. Scarce outcrops of welded tuff suggest that the avalanche was followed by the emission of dacitic ignimbrites (66 wt % SiO_2).

Second episode of construction (NCAY-MS5). On the northern flank of Cayambe, this unit consists of at least three 100 m thick lava flows of andesite, bearing amphibole and pyroxene (61–63 wt % SiO_2; the Las Antenas lava flows, Fig. 3). These lava flows overlie the Río San Pedro debris avalanche deposits. Above 4600 m altitude, the upper part of this series contains block-and-ash layers. The blocks are of Pl + Amph + Cpx + Opx + Mag ± Bt bearing dacite; this attests to the presence of new dacite domes (64–65 wt % SiO_2) in the summit area.

On the southern flank, a 200–250 m thick sequence of lava flows (e.g. La Dormida lava flows, Fig. 3) overlie lavas from NCAY-MS1 unit or directly rest on the metamorphic basement. They consist of amphibole-bearing andesites and dacites (62–65 wt % SiO_2). At 4300 m in the La Dormida valley, three inclusion-rich lava flows form a remarkable sequence. Within each flow, the size (millimetric to decimetric) and percentage of the magmatic inclusions (5–50%) increase from the base to the top in such a manner that the rock looks like a breccia resulting from mingling processes. We interpret the lavas as the result of mixing of a host porphyritic dacite (64 wt % SiO_2) and an aphyric andesitic magma (58–60 wt % SiO_2). Two $^{40}Ar/^{39}Ar$ whole-rock dates obtained from 'Las Antenas' and 'La Dormida' lava flows give plateau ages of 100 ± 4 and 95 ± 5 ka (Table 1; Fig. 3).

The La Chimba ignimbrite (NCAY-MS6). A welded deposit, 60–80 m thick (Fig. 3), containing blocks of amphibole-rich dacite (64–65 wt % SiO_2) is found on the northwestern flank of the complex, partially filling the La Chimba valley. This deposit ends the second period of dome construction and is covered by large moraines emplaced during the last glacial maximum (11–14 ka; Clapperton, 1993).

The Nevado Cayambe secondary summit (NCAY-SS) and the recent activity

The younger edifice of CVC is a small (~10 km^3) stratocone, capped by a summit dome complex (NCAY-SS). It grew on the eastern flank of NCAY-MS cone and its deposits are free of glacial erosion, suggesting a Holocene age. This edifice (NCAY-SS1; 58–66 wt % SiO_2) is characterized by andesitic effusive activity, which turned to more explosive activity, related to the dacitic summit dome complex. Recent eruptive activity appears restricted to the last 4000 years. Three periods of strong pyroclastic activity were separated by quiescent episodes of 600–900 years (Samaniego *et al.*, 1998). At least four notable block-and-ash flow sequences were generated, which are related to recent domes (NCAY-SS2, NCAY-SS3, Fig. 3). Light and dark grey banded blocks and bombs from these units have a large compositional range, from andesite to dacite (59–66 wt % SiO_2) and contain Pl + Amph + Cpx + Opx + Mag ± Bt.

The 'Cono La Virgen'

This satellite cone (1·5 km in diameter and 400 m high) is located 8 km from the main summit, on the lower eastern slope of the complex. As it lacks evidence of glacial erosion, its activity may have been contemporaneous with that of the present summit dome complex. This cone emitted a 250–300 m thick sequence of lava flows (CLV, 'Planada de La Virgen lava flows', Fig. 3), the estimated volume of which is about 3–4 km^3. These rocks are porphyritic andesites (59–60 wt % SiO_2), with a mineralogy consisting of Pl + Amph + Opx + Cpx + Bt + Ol + Mag.

CHARACTERIZATION OF CAYAMBE VOLCANIC ROCKS

Mineralogy

Mineral compositions of 30 rocks have been analysed by electron microprobe at the Laboratoire Magmas et Volcans, Université Blaise Pascal, Clermont-Ferrand, France (13 sections using a CAMECA Camebax and 17 sections with a CAMECA SX-100). In both cases, the operating conditions were 15 kV accelerating voltage, 10–12 nA beam current and 10 s counting time. Tables 2–5 present selected phenocryst compositions for representative rocks from the different volcanic units. The complete dataset is available for downloading

Table 2: Selected plagioclase compositions (in wt %) for lavas of CVC

Edifice:	VCAY							NCAY-ANG		NCAY-MS			NCAY-SS										CLV					
Sample:	CAY48		CAY66			CAY31		CAY89		CAY169			CAY44B			CAY4C		CAY4C			CAY2E			CAY45A		CAY45A		CAY45C	
	C	R	C	I-a	R	C	R	C-a	R	C	I-a	R	C	I-a	R	C	R	C	I-a	R	C	I	R	C	R	C	R	C	R
SiO_2	53·11	57·03	56·36	51·29	54·81	53·71	60·35	48·80	59·00	56·54	60·60	49·82	60·56	55·53	52·78	59·66	51·11	54·23	50·59	50·16	51·31	54·77	58·44	58·84	57·01	51·48	56·85	58·51	60·06
TiO_2	0·09	0·09	0·07	0·00	0·07	0·08	0·02	0·06	0·04	0·02	0·18	0·05	0·00	0·10	0·00	0·02	0·11	0·08	0·00	0·12	0·00	0·08	0·00	0·06	0·07	0·01	0·00	0·04	0·08
Al_2O_3	28·98	25·80	26·49	30·13	28·27	28·38	23·79	33·31	25·54	25·93	22·68	30·66	24·11	28·05	29·23	24·82	30·17	28·51	30·56	31·39	30·46	28·87	26·38	24·90	25·84	29·57	26·28	26·35	24·84
Cr_2O_3	0·00	0·01	0·00	0·00	0·00	0·05	0·00	0·00	0·03	0·00	0·01	0·00	0·00	0·06	0·02	0·00	0·02	0·00	0·01	0·00	0·00	0·00	0·00	0·00	0·02	0·00	0·03	0·01	0·06
FeO*	0·57	0·68	0·66	0·67	0·70	0·36	0·20	0·32	0·31	0·16	1·22	0·63	0·15	0·64	0·72	0·29	0·80	0·36	0·48	1·76	0·36	0·25	0·29	0·30	0·28	0·24	0·25	0·15	0·24
MnO	0·00	0·00	0·00	0·02	0·03	0·06	0·00	0·00	0·00	0·00	0·00	0·01	0·03	0·00	0·12	0·00	0·00	0·00	0·03	0·05	0·02	0·00	0·06	0·00	0·07	0·00	0·00	0·00	0·04
MgO	0·08	0·05	0·06	0·03	0·07	0·01	0·03	0·04	0·02	0·02	0·13	0·06	0·04	0·04	0·06	0·06	0·11	0·06	0·07	0·06	0·03	0·04	0·04	0·00	0·01	0·03	0·01	0·03	0·04
NiO	0·00	0·02	0·00	0·00	0·00	0·00	0·08	0·01	0·00	0·00	0·02	0·00	0·00	0·00	0·00	0·00	0·09	0·00	0·09	0·00	0·00	0·00	0·00	0·01	0·01	0·00	0·01	0·00	0·06
CaO	11·71	8·63	9·64	13·35	11·22	10·54	5·55	16·48	7·78	8·61	8·26	14·70	6·07	10·92	11·89	6·65	12·86	10·68	13·56	14·65	12·75	10·63	7·86	6·98	8·09	12·90	8·81	8·09	6·65
Na_2O	4·80	6·57	6·29	3·86	5·15	4·90	7·49	2·41	6·75	6·47	4·74	3·16	7·23	4·65	4·28	6·96	3·73	4·99	3·80	3·15	3·74	5·11	6·39	6·70	6·06	4·17	6·00	6·31	6·60
K_2O	0·32	0·61	0·55	0·17	0·32	0·24	1·04	0·07	0·77	0·41	0·63	0·17	0·64	0·39	0·27	0·58	0·16	0·20	0·11	0·09	0·16	0·22	0·44	0·85	0·57	0·21	0·61	0·42	1·14
Total	99·65	99·49	100·11	99·53	100·64	98·32	98·55	101·50	100·22	98·16	98·46	99·28	98·83	100·40	99·35	99·05	99·15	99·11	99·31	101·42	98·83	99·97	99·89	98·64	98·04	98·62	98·85	99·92	99·82
An %	56·39	40·61	44·47	65·03	53·63	53·54	27·28	78·80	37·22	41·36	46·97	71·27	30·48	55·17	59·59	33·36	64·94	53·55	65·93	71·60	64·70	52·79	39·41	34·69	40·99	62·33	43·21	40·43	33·34
Ab %	41·79	55·95	52·48	33·98	44·56	45·02	66·63	20·83	58·41	56·29	48·75	27·75	65·69	42·50	38·80	63·18	34·09	45·27	33·43	27·87	34·35	45·90	57·98	60·27	55·56	36·45	53·21	57·07	59·86
Or %	1·83	3·44	3·05	0·99	1·81	1·45	6·09	0·37	4·37	2·35	4·28	0·98	3·83	2·33	1·61	3·46	0·97	1·18	0·64	0·53	0·95	1·31	2·62	5·04	3·44	1·22	3·58	2·50	6·80

C, core; I, interior; R, rim; a, altered.

Table 3: Selected pyroxene compositions (in wt %) for lavas of CVC

Edifice:	VCAY							NCAY-ANG		NCAY-MS		NCAY-SS				CLV	
Sample:	CAY56			CAY48		CAY66		CAY77A		CAY168D		CAY44B		CAY44C		CAY45C	
	C	I	R	C	R	C	R	C	R	C	R	C	R	C	R	C	R
SiO_2	51·56	50·29	51·16	50·88	51·68	50·72	50·05	51·36	52·65	50·59	50·22	51·19	49·11	48·27	51·50	53·72	52·90
TiO_2	0·69	0·67	0·85	0·68	0·55	0·63	0·63	0·67	0·37	0·50	0·67	0·37	0·89	0·81	0·37	0·21	0·46
Al_2O_3	2·21	2·36	2·50	2·49	4·07	3·14	2·14	4·08	1·87	3·44	3·84	4·09	6·24	5·76	2·42	1·07	1·09
Cr_2O_3	0·00	0·05	0·00	0·06	0·19	0·34	0·00	0·30	0·17	0·55	0·43	0·52	0·00	0·07	0·15	0·69	0·04
FeO*	10·42	12·43	10·63	12·97	7·01	11·25	14·04	8·51	7·79	6·80	7·65	7·05	8·70	9·04	7·71	3·09	4·98
MnO	0·26	0·36	0·22	0·28	0·16	0·27	0·32	0·18	0·21	0·15	0·19	0·20	0·14	0·13	0·17	0·11	0·12
MgO	16·13	14·45	15·31	12·67	16·14	14·34	13·53	14·66	16·57	15·93	15·80	15·21	13·63	13·76	16·09	18·25	16·85
NiO	0·00	0·02	0·01	0·02	0·01	0·02	0·00	0·05	0·00	0·03	0·00	0·23	0·07	0·00	0·03	0·05	0·00
CaO	18·77	18·61	18·55	18·39	19·66	19·39	18·14	20·20	20·10	20·03	19·80	19·45	19·59	18·94	19·57	20·40	21·38
Na_2O	0·34	0·45	0·37	0·53	0·38	0·47	0·48	0·50	0·28	0·41	0·29	0·57	0·51	0·47	0·37	0·37	0·19
K_2O	0·00	0·00	0·02	0·00	0·01	0·00	0·00	0·00	0·00	0·00	0·00	0·00	0·00	0·02	0·04	0·02	0·00
Total	100·38	99·59	99·61	98·97	99·85	100·57	99·33	100·49	100·01	98·43	98·89	98·89	98·86	97·27	98·42	97·97	98·02
En %	45·28	41·35	44·07	38·02	47·04	41·25	39·08	43·02	46·69	46·53	45·86	45·72	41·69	42·32	46·55	52·59	48·02
Fs %	16·85	20·37	17·56	22·32	11·72	18·59	23·27	14·34	12·63	11·41	12·77	12·26	15·19	15·79	12·78	5·13	8·16
Wo %	37·88	38·28	38·37	39·66	41·24	40·16	37·65	42·64	40·68	42·06	41·36	42·03	43·12	41·89	40·68	42·27	43·82
mg-no.	73·37	67·62	71·94	63·52	80·42	69·41	63·19	75·42	79·11	80·67	78·64	79·30	73·37	73·10	78·87	91·36	85·79

Edifice:	VCAY						NCAY-ANG		NCAY-MS				NCAY-SS		CLV	
Sample:	CAY56		CAY48		CAY31		CAY77A		CAY168B		CAY1A		CAY44B		CAY45C	
	C	R	C	R	C	R	C	R	C	R	C	R	C	R	C	R
SiO_2	52·98	53·70	51·35	52·49	52·64	51·90	54·45	54·11	51·55	53·26	54·07	54·01	54·63	53·32	53·78	54·23
TiO_2	0·38	0·42	0·32	0·30	0·16	0·16	0·05	0·22	0·08	0·20	0·20	0·29	0·13	0·14	0·18	0·06
Al_2O_3	1·48	1·57	1·40	0·94	1·15	0·71	2·72	2·62	0·88	2·13	2·50	2·03	2·26	3·11	0·92	0·65
Cr_2O_3	0·05	0·05	0·08	0·02	0·05	0·03	0·65	0·24	0·02	0·12	0·22	0·07	0·25	0·29	0·00	0·00
FeO*	19·09	17·04	25·79	20·92	21·71	26·39	11·43	14·32	21·94	14·33	13·01	16·03	14·47	13·25	20·65	21·05
MnO	0·37	0·24	0·59	0·45	0·97	1·14	0·22	0·32	1·21	0·28	0·32	0·33	0·30	0·63	0·98	0·75
MgO	24·15	25·51	18·99	22·32	22·61	18·92	29·11	27·04	22·57	26·65	27·47	25·80	26·85	27·55	23·21	24·25
NiO	0·01	0·04	0·01	0·00	0·00	0·04	0·05	0·07	0·00	0·04	0·00	0·06	0·03	0·04	0·00	0·01
CaO	1·93	2·27	1·71	1·67	0·81	0·81	1·76	1·56	0·63	2·02	1·47	1·26	1·84	1·41	0·71	0·64
Na_2O	0·05	0·03	0·05	0·06	0·01	0·00	0·12	0·05	0·05	0·01	0·05	0·01	0·17	0·29	0·00	0·04
K_2O	0·00	0·00	0·00	0·00	0·00	0·01	0·00	0·02	0·04	0·00	0·00	0·05	0·00	0·08	0·00	0·00
Total	100·49	100·88	100·30	99·17	100·12	100·12	100·56	100·57	98·97	99·03	99·30	99·93	100·94	100·11	100·44	101·68
En %	66·25	69·24	54·20	62·85	62·93	54·13	78·86	74·30	62·65	73·38	76·27	71·90	73·64	75·78	64·70	65·60
Fs %	29·92	26·31	42·26	33·77	35·46	44·20	17·74	22·60	36·11	22·60	20·78	25·57	22·74	21·43	33·88	33·15
Wo %	3·83	4·44	3·54	3·38	1·61	1·66	3·40	3·10	1·24	4·02	2·95	2·53	3·62	2·80	1·42	1·25
mg-no.	69·28	72·73	56·75	65·53	64·99	56·11	81·94	77·09	64·70	76·82	79·01	74·16	76·78	78·85	66·70	67·21

C, core; I, interior; R, rim.

from http://www.petrology.oupjournals.org. The striking mineralogical difference between the ancient and the modern volcano is the ubiquitous presence of amphibole in the NCAY rocks, which have the assemblage Pl + Amph + Cpx + Opx + Mag, whereas amphibole is accessory or absent in the VCAY rocks, the mineral assemblage of which is dominantly Pl + Cpx + Opx + Mag.

Plagioclase

Plagioclase is the most abundant phenocryst phase in all of the Cayambe rocks (10–25 vol. %). In VCAY lavas, phenocrysts ($An_{27–76}$; Fig. 4) are generally euhedral with normal (e.g. $An_{54–27}$, $An_{56–41}$; Table 2) and reverse (e.g. $An_{44–65–53}$) zoning. Some phenocrysts have dusty concentric zones. In NCAY rocks, the plagioclase phenocryst

Table 4: Selected amphibole and biotite compositions (in wt %) for lavas of CVC

	Amphibole															Biotite									
Edifice:	VCAY		NCAY-ANG				NCAY-MS			NCAY-SS				CLV		NCAY-ANG		NCAY-MS		NCAY-SS		CLV			
Sample:	CAY107		CAY77A		CAY80A	CAY89	CAY169	CAY29	CAY97A	CAY44C	CAY3B2	CAY4C		CAY45A		CAY80A	CAY15	CAY41A				CAY45C			
	C	R	C	R	C	C	C	C	C	C	C	C	R	C	I	C	R	C	R	C	R	C	R	R	R
SiO_2	42·24	42·69	47·40	48·70	40·12	44·37	41·93	41·82	47·83	40·29	42·84	47·28	47·56	42·02	43·14	36·84	36·61	37·15	37·52	37·08	38·08	38·54	38·55	37·84	38·05
TiO_2	2·82	2·31	1·45	1·55	4·14	2·70	2·70	2·59	1·31	3·10	1·66	1·39	1·37	2·77	2·64	4·53	4·53	5·11	5·06	4·44	4·28	2·64	2·01	4·48	4·40
Al_2O_3	12·15	11·72	7·25	6·84	13·16	9·97	11·82	12·69	6·86	13·61	12·00	7·24	6·75	11·23	10·50	13·53	13·32	14·14	13·92	14·43	14·70	14·52	14·78	14·08	13·90
Cr_2O_3	0·01	0·02	0·04	0·02	0·03	0·03	0·03	0·03	0·03	0·00	0·11	0·00	0·13	0·05	0·00	0·02	0·00	0·00	0·22	0·00	0·00	0·06	0·84	0·00	0·00
FeO*	12·50	13·26	14·46	12·10	12·61	12·10	11·85	10·66	12·75	12·71	12·84	11·83	11·15	11·75	11·57	16·10	15·99	13·52	13·45	13·91	13·51	6·45	6·17	9·07	7·69
MnO	0·20	0·19	0·45	0·37	0·10	0·28	0·18	0·09	0·34	0·15	0·42	0·44	0·33	0·08	0·17	0·26	0·19	0·08	0·07	0·12	0·15	0·06	0·08	0·07	0·08
MgO	14·04	13·44	13·74	15·84	13·64	14·79	14·37	14·96	14·68	12·69	14·00	15·44	15·89	14·72	15·79	0·01	0·01	0·00	0·01	0·09	0·05	0·07	0·01	0·07	0·03
NiO	0·02	0·03	0·00	0·00	0·00	0·01	0·01	0·01	0·00	0·02	0·11	0·06	0·02	0·00	0·06	13·68	13·82	14·82	15·53	15·56	15·71	21·33	21·56	18·06	19·12
CaO	11·39	11·71	11·21	11·14	10·44	11·44	11·03	11·18	11·17	10·50	11·21	10·67	10·97	11·43	11·13	0·00	0·02	0·01	0·01	0·00	0·03	0·04	0·07	0·00	0·02
Na_2O	2·63	2·62	1·44	1·45	2·41	2·62	2·34	2·74	1·43	2·77	2·18	1·33	1·32	2·49	2·29	0·64	0·70	0·69	0·68	0·83	0·87	0·58	0·59	0·78	0·72
K_2O	0·61	0·61	0·63	0·57	0·62	0·59	0·50	0·61	0·50	0·51	0·44	0·43	0·42	0·97	0·92	9·11	8·97	8·57	9·07	8·58	8·20	9·54	9·70	8·83	9·24
Total	98·59	98·61	98·07	98·59	97·27	98·90	96·75	97·38	96·90	96·36	97·81	96·11	95·91	97·71	98·20	94·72	94·16	94·09	95·54	95·04	95·58	93·83	94·36	93·28	93·25
mg-no.	66·70	64·37	62·89	70·00	65·84	68·54	68·36	71·44	67·24	64·03	66·03	69·94	71·75	69·08	70·86	60·22	60·63	66·14	67·29	66·59	67·45	85·49	86·16	78·01	81·59

C, core; I, interior; R, rim.

Table 5: Selected olivine and Fe–Ti oxide compositions (in wt %) for lavas of CVC

	Olivine								Fe–Ti oxides									
Edifice:	NCAY-MS		NCAY-SS		CLV				VCAY			NCAY-ANG		NCAY-MS		NCAY-SS		CLV	
Sample:	CAY169				CAY4C		CAY45A	CAY45C	CAY56	CAY107		CAY89		CAY169		CAY2E		CAY45C	
	C	R	C	R	C	R		C R	C	C	C	C	C	C	C	C	C	C	C
Mineral:									Ti-Mag	Ti-Mag	Ilm	Ti-Mag	Ilm	Ti-Mag	Ilm	Ti-Mag	Ilm	Ti-Mag	Ilm
SiO_2	39·32	38·77	38·34	38·44	39·93	39·13	39·96	39·32	0·05	0·60	0·04	0·03	0·01	0·12	0·03	0·10	0·04	0·10	0·00
TiO_2	0·00	0·00	0·02	0·00	0·03	0·04	0·00	0·00	12·47	14·13	49·49	8·10	44·06	10·08	44·53	5·47	37·25	6·01	32·15
Al_2O_3	0·02	0·03	0·02	0·02	0·02	0·05	0·03	0·05	4·12	1·29	0·12	1·31	0·11	1·94	0·18	1·96	0·22	1·76	0·44
Cr_2O_3	0·01	0·03	0·13	0·06	0·00	0·06	0·00	0·04	0·81	0·23	0·00	0·09	0·02	0·03	0·06	0·08	0·00	0·19	0·03
FeO*	15·16	18·98	22·87	23·56	12·70	15·34	13·86	16·86	74·37	75·74	48·18	83·71	52·30	78·58	51·16	85·20	58·06	82·94	59·67
MnO	0·25	0·33	0·27	0·32	0·21	0·25	0·27	0·37	0·31	0·14	0·52	0·34	0·55	0·28	0·39	0·57	0·51	0·38	0·28
MgO	44·84	41·50	38·55	38·10	46·92	45·28	44·82	43·10	2·79	0·39	1·49	0·56	1·58	1·59	2·50	1·56	2·15	0·02	2·60
NiO	0·11	0·09	0·04	0·13	0·16	0·10	0·04	0·15	0·03	0·03	0·02	0·00	0·00	0·00	0·01	0·03	0·06	2·22	0·00
CaO	0·18	0·19	0·15	0·11	0·17	0·18	0·15	0·15	0·10	0·01	0·06	0·02	0·01	0·16	0·00	0·47	0·06	0·01	0·00
Na_2O	0·04	0·02	0·03	0·00	0·11	0·00	0·00	0·00	0·00	0·00	0·00	0·00	0·00	0·00	0·00	0·00	0·00	0·00	0·00
K_2O	0·01	0·00	0·03	0·04	0·01	0·00	0·00	0·00	0·00	0·02	0·01	0·00	0·03	0·03	0·00	0·10	0·06	0·03	0·03
Total	99·93	99·91	100·45	100·77	100·26	100·43	99·12	100·06	95·05	92·56	99·91	94·16	98·68	92·80	98·86	95·54	98·41	93·66	95·2
mg-no.	84·05	79·58	75·02	74·24	86·81	84·02	85·21	82·00											

C, core; I, interior; R, rim.

composition has a similar range ($An_{25–79}$), and textures such as reaction rims and dusty concentric zones or cores are abundant (maximum 30% of phenocrysts). The composition of these dusty zones is generally more calcic. Many phenocrysts are euhedral with normal (e.g. $An_{79–34}$, $An_{65–39}$) or reverse (e.g. $An_{41–71}$, $An_{27–60}$; see arrows in Fig. 4) zoning, but some large phenocrysts with oscillatory zoning (e.g. $An_{33–65–54–66–72}$) are also observed. In CLV lavas, plagioclase ($An_{31–68}$) is generally euhedral, without alteration, and with normal zoning (e.g. $An_{62–43}$, $An_{40–33}$), though scarce reverse zoning (e.g. $An_{40–64}$) also exists. Although it has the same An content, the plagioclase of the VCAY and CLV rocks has higher Or contents than the NCAY plagioclase (Fig. 4), probably because it crystallized from magma richer in K.

Clinopyroxene

In VCAY andesites, clinopyroxene of augitic composition (Morimoto *et al.*, 1988) is present in amounts up to 10–15 vol. %, whereas it is an accessory phase or is absent in the dacites (<2 vol. %). Typical augite phenocrysts are euhedral or subhedral with reverse zoning (e.g. *mg*-number 64–80; Fig. 5a; Table 3) [*mg*-number = $100Mg/(Mg + Fe^t)$ in mol %, where Fe^t is total iron, as Fe^{2+}]. Rare phenocrysts with normal or oscillatory zoning have been also observed (e.g. *mg*-number 69–63; *mg*-number 73–68–72). In NCAY lavas, clinopyroxene (<1 vol. %) varies from diopside to augite and shows reverse zoning (e.g. *mg*-number 73–78), but some normally zoned crystals (e.g. *mg*-number 79–73) or without zoning also exist. Clinopyroxenes from CLV andesites (2–3 vol. %) are augite and diopside, euhedral and normally zoned (e.g. *mg*-number 91–86).

NCAY clinopyroxenes show a narrower range in MgO (*mg*-number 71–84) than VCAY pyroxenes (*mg*-number 61–82), and the most Mg-rich crystals are found in the CLV rocks (*mg*-number 80–91). Additionally, some NCAY and CLV clinopyroxenes are also Cr_2O_3-rich (up to 1 wt %) compared with VCAY clinopyroxenes (Cr_2O_3 <0·4 wt %). These high *mg*-numbers and Cr_2O_3 contents suggest that these minerals crystallized from more primitive magmas.

In addition, clinopyroxene from the CVC exhibits a large range of Al_2O_3 contents (Fig. 5a). In VCAY clinopyroxenes, *mg*-number and Al_2O_3 are positively correlated. In contrast, NCAY clinopyroxene has a maximum Al_2O_3 (6–7 wt %) at a *mg*-number of 70–73.

Orthopyroxene

Enstatite ($En_{54–79}$) is common in all CVC rocks. In VCAY lavas, most orthopyroxene phenocrysts (5–10 vol. %; *mg*-number 56–82) are euhedral, without zoning, but

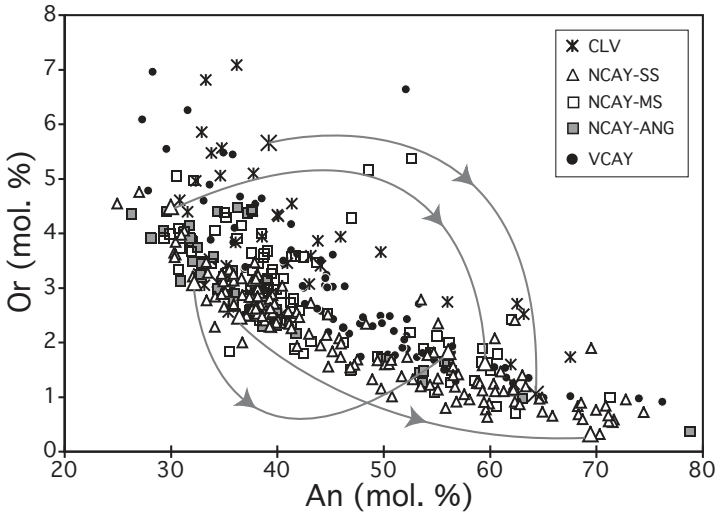

Fig. 4. Composition of plagioclase in CVC rocks plotted as Or (mol %) vs An (mol %). Arrows represent strong core-to-rim inverse zoning in plagioclases from the NCAY-SS and CLV edifices. Abbreviations are as in Fig. 3.

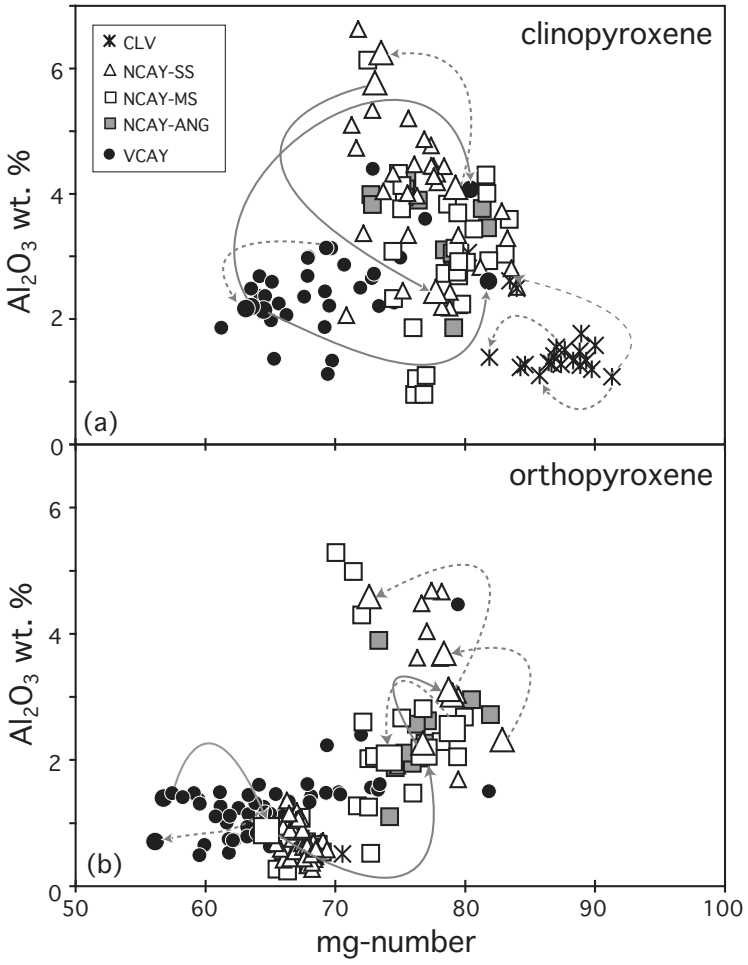

Fig. 5. Composition of (a) clinopyroxene and (b) orthopyroxene plotted as Al_2O_3 wt % vs *mg*-number. Arrows represent strong core-to-rim inverse (continuous line) or normal (dotted line) zoning in pyroxenes.

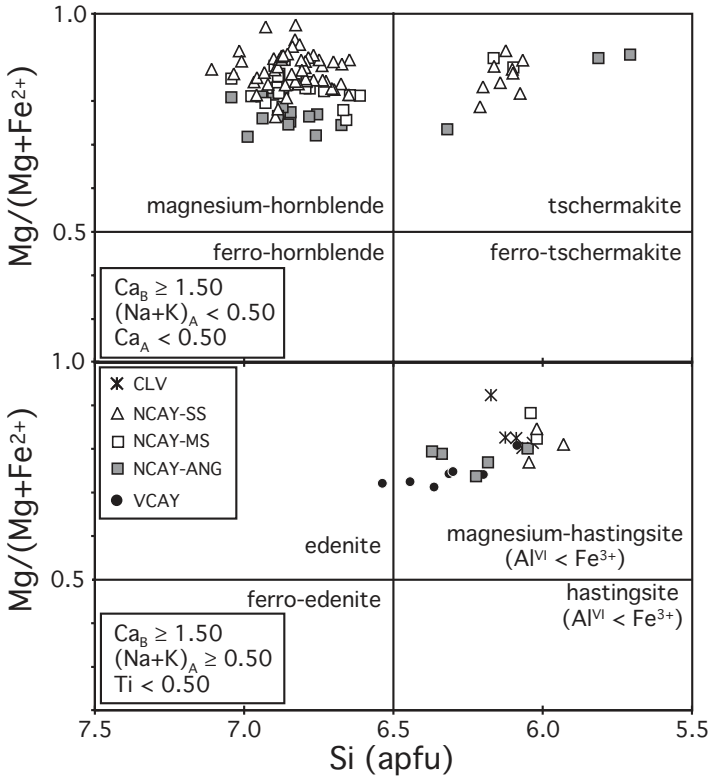

Fig. 6. Amphibole classification (after Leake *et al.*, 1997) expressed by $Mg/(Mg + Fe^{2+})$ vs Si (a.p.f.u., atoms per formula unit) diagram.

some phenocrysts are normally (e.g. *mg*-number 65–56; Table 3) or reversely zoned (e.g. *mg*-number 57–66). NCAY orthopyroxene (<10 vol. %) is of two compositional types: a homogeneous Mg-poor group (*mg*-number 65–69), with unzoned crystals; and a more heterogeneous Mg-rich group (*mg*-number 70–83), which exhibits normal (e.g. *mg*-number 82–77) and reverse zoning (e.g. *mg*-number 65–77). Crystals from both groups are frequently present in the same rock, but individual minerals with zoning between these compositions are rare. The CLV orthopyroxene (2–3 vol. %; *mg*-number 67–71) is homogeneous.

As for clinopyroxene, orthopyroxene from the CVC displays large variations in an Al_2O_3 vs *mg*-number diagram (Fig. 5b). VCAY and most NCAY orthopyroxenes show an Al_2O_3 decrease correlated with *mg*-number decrease; however, some NCAY orthopyroxenes are Al-rich (4–5 wt %) at a *mg*-number of 70–78.

Amphibole

Amphibole appears as accessory phase in VCAY rocks (<1 vol. %). When present, it consists of magnesium-hastingsite or edenite crystals (Fig. 6; Leake *et al.*, 1997) with rounded rims. In NCAY rocks, and particularly in dacites, magnesium-hornblende, with some tschermakite and magnesium-hastingsite (Fig. 6), is the most important mafic mineral, although it never exceeds 10 vol. %. It commonly occurs as transparent, euhedral phenocrysts, but crystals with altered rims or completely altered crystals are also abundant. CLV amphiboles (8–10 vol. %) are magnesium-hastingsite, and are (except for a few cores) completely altered. In contrast to pyroxenes, *mg*-numbers for the rare VCAY and CLV amphiboles fall in a narrow range (63–67 and 67–71, respectively) and even in NCAY, the range of Mg-numbers in amphibole is small (62–72).

Two alteration types were recognized in NCAY amphibole: (1) most frequent is a 'black-type' of alteration, in which amphibole is completely replaced by an aggregate of Fe–Ti oxides and pyroxenes (opacite); and (2) a rare (<5% total amphibole) 'gabbroic-type' of alteration, characterized by replacement of amphibole by an assemblage of Opx + Cpx + Pl + Mag. Following Garcia & Jacobson (1979), we suggest that these features reflect either oxidation after lava emplacement (black-type) or dehydration during magma ascent (gabbroic-type). Alternatively, Nixon (1988) suggested that amphibole can decompose by 'solid-state dehydration reactions' induced by superheating of low temperature magmas, when evolved magma mixes with hotter (more mafic?) magma.

Two main amphibole compositional groups can be distinguished (Table 4): (1) low Al_{tot}, (Na + K) and

Ti amphiboles, corresponding to the magnesium-hornblende of NCAY; and (2) high Al_{tot}, (Na + K) and Ti amphiboles, corresponding to the magnesium-hastingsite encountered in all units. A subordinate group corresponds to the rare tschermakite crystals observed in the NCAY rocks.

Biotite

Biotite phenocrysts characterize NCAY-ANG dacites (<5 vol. %) and CLV andesites (1–2 vol. %). Some biotite phenocrysts have Fe–Ti oxide reaction rims. CLV biotite is Mg-rich and Ti-poor (*mg*-number 78–88; 2·0–4·6 wt % TiO_2; Table 4), compared with NCAY biotite (*mg*-number 56–72; 4·2–5·3 wt % TiO_2).

Fe–Ti oxides

In all CVC rocks, Fe–Ti oxides appear as microphenocrysts and microlites within the matrix (<2–3 vol. %; Table 5), as well as inclusions in other phases (pyroxenes, amphibole or plagioclase). Magnetite is ubiquitous, whereas ilmenite is an accessory mineral in the NCAY rocks.

Olivine

Olivine (<2 vol. %) is present in andesites from the CLV cone, and occurs exceptionally in NCAY rocks (<1 vol. %). CLV olivine phenocrysts ($Fo_{81–87}$; Table 5) are subhedral and do not show any zoning. Most olivines from the NCAY rocks ($Fo_{74–84}$) show disequilibrium features, such as skeletal or resorbed crystals and reaction rims (composed of pyroxene, plagioclase and Fe–Ti oxides), suggesting that these crystals are xenocrysts.

Geochemical characteristics

Major and trace element concentrations in 178 whole-rock samples were measured at the Laboratoire de Pétrologie de l'Université de Bretagne Occidentale (Brest, France). The method used was inductively coupled plasma atomic emission spectrometry, except for Rb, which was determined by atomic emission spectrometry (see Cotten *et al.*, 1995 for details). Sr and Nd isotopic ratios were measured at the Laboratoire Magmas et Volcans, Université Blaise Pascal (Clermont-Ferrand, France) on 16 rocks (see Dosso *et al.*, 1991 for the analytical method). A selection of these whole-rock analyses and all isotopic determinations are presented in Table 6. The entire dataset is available as an electronic appendix, which may be downloaded from http://www.petrology.oupjournals.org.

Major and trace elements

In CVC rocks, SiO_2 ranges from 57 to 69 wt % (Fig. 7). The rocks define a single medium-K magmatic trend in the K_2O vs SiO_2 diagram (modified from Peccerillo & Taylor, 1976). Basalts and basaltic andesite compositions are absent, and only two samples from the older VCAY edifice are rhyolites (72–73 wt % SiO_2). CLV lavas plot separately in the high-K andesite field, contrasting with all other volcanic rocks from the complex (Fig. 7).

VCAY consists of: (1) an andesitic group (57·3–63·1 wt % SiO_2), which is volumetrically significant, as it mainly corresponds to the VCAY1 sequence of lava flows; and (2) a silicic group (64·8–72·8 wt % SiO_2), which is less significant in volume and corresponds to late volcanic products (VCAY2 and 3). For VCAY lavas, large ion lithophile elements (LILE), high field strength elements (HFSE) and light rare earth elements (LREE) are positively correlated with silica, but some scattering is observed for HFSE and LREE. In contrast, middle rare earth elements (MREE) and heavy rare earth elements (HREE) show no correlation with silica, although maximum values are observed for samples with 61–64 wt % SiO_2. Ni, V and, to a lesser extent, Sr exhibit negative correlations with silica (Fig. 7).

All NCAY lavas form a single series, without strong differences between the three successive edifices, except for a wide dispersion in Na_2O and REE for the NCAY-ANG rocks. At a given SiO_2 content, NCAY lavas are slightly enriched in MgO, Ni and Cr compared with VCAY rocks. Also, NCAY lavas have lower K_2O/Na_2O than VCAY rocks (Fig. 7; Tables 6 and 7). Trace elements emphasize the differences between the older and younger edifices: NCAY lavas are systematically poorer in LILE, HFSE, LREE and especially HREE. For all NCAY units, LILE, HFSE and LREE concentrations increase with SiO_2 content (Fig. 7). Conversely, Sr, MREE, HREE and Y concentrations decrease with SiO_2, but to a smaller extent than Ni and V. In Harker diagrams, Ni concentrations are scattered (as well as Cr), with a wide range in Ni contents (up to a factor of 7), suggesting a more complex petrogenetic process than simple fractional crystallization.

The high-K CLV andesites (59·3–59·9 wt % SiO_2) are slightly enriched in MgO and depleted in Al_2O_3 compared with other CVC rocks. Their most striking characteristic is very high LILE and LREE contents, whereas HFSE and HREE (and Y) concentrations are in the same range of variation as other CVC rocks.

Plots of $(La/Yb)_N$ vs Yb_N and Sr/Y vs Y highlight the differences between the NCAY and VCAY rocks (Fig. 8; Table 7). These diagrams clearly separate (1) a 'classical' calc-alkaline series consisting of VCAY rocks, and (2) an 'adakitic' series corresponding to the younger NCAY volcano. In addition, as is typical for adakitic suites where mafic rocks are absent (Defant & Drummond, 1990; Martin, 1999), basalts are absent in the CVC, and the lavas are Al_2O_3-rich (Al_2O_3 > 15 wt % for SiO_2 = 70 wt %).

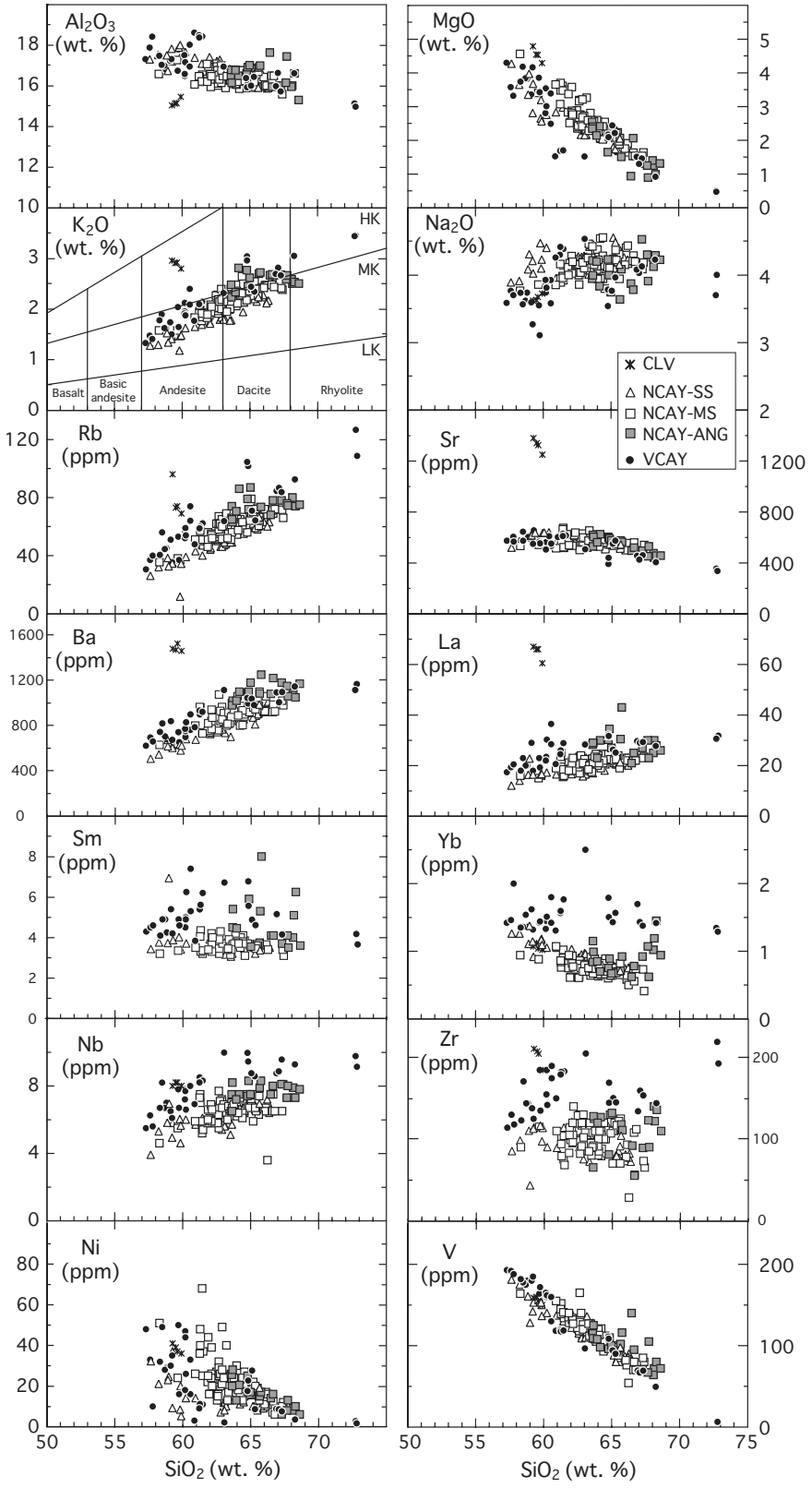

Fig. 7. Variation diagrams for selected major and trace elements. The subdivision shown in the K_2O vs SiO_2 diagram is modified from Peccerillo & Taylor (1976).

Table 6: Selected whole-rock analyses of CVC lavas

Edifice:	VCAY									NCAY-ANG			
Sample:	CAY56	CAY102	CAY55B	CAY66	CAY109B	CAY106B	CAY107	CAY31	CAY147A1	CAY28C	CAY80A	CAY78A	CAY89
SiO_2	56·50	57·70	58·30	59·40	59·80	61·00	64·50	66·80	69·80	62·55	64·00	64·50	68·50
TiO_2	0·88	0·88	0·92	0·87	0·82	0·85	0·68	0·51	0·29	0·69	0·63	0·67	0·48
Al_2O_3	17·08	17·30	17·05	17·29	17·80	18·30	15·90	16·30	14·40	16·25	16·98	16·67	15·28
Fe_2O_3*	7·67	6·90	6·38	7·05	6·15	5·43	5·15	3·45	1·89	5·24	4·11	4·11	3·82
MnO	0·11	0·10	0·09	0·08	0·07	0·06	0·06	0·07	0·07	0·06	0·02	0·05	0·07
MgO	4·24	3·70	4·10	2·77	2·46	1·69	2·11	0·92	0·47	2·50	0·90	1·48	1·31
CaO	7·08	6·70	6·70	5·30	5·19	5·17	4·25	2·50	1·70	4·50	3·15	3·75	3·50
Na_2O	3·54	3·70	3·22	3·88	3·88	4·36	3·78	4·15	3·85	3·88	3·73	4·01	4·22
K_2O	1·31	1·76	1·48	1·89	2·37	2·13	2·96	3·00	3·32	2·44	2·57	2·67	2·50
P_2O_5	0·21	0·20	0·21	0·20	0·21	0·25	0·17	0·17	0·08	0·22	0·18	0·17	0·16
LOI	1·21	0·82	1·77	1·02	1·06	0·91	0·52	1·18	3·71	1·21	3·48	1·79	0·26
Total	99·83	99·76	100·22	99·75	99·81	100·15	100·08	99·05	99·58	99·54	99·75	99·87	100·10
Sc	18·5	15·8	16·0	15·1	12·5	10·7	10·8	5·6	1·9	9·4	9·0	8·4	6·3
V	193	182	185	165	130	119	110	50	7	115	140	116	72
Cr	68	83	98	24	39	19	58	6	6	54	55	44	11
Co	27·0	22·0	20·0	19·0	14·0	11·0	12·0	6·0	5·0	18·0	10·0	13·0	7·0
Ni	48·0	32·0	35·0	18·0	16·0	11·0	23·0	4·0	2·0	25·5	14·0	17·0	6·0
Rb	30·5	40·5	35·5	52·0	74·0	62·0	102·0	93·0	109·0	74·0	68·0	73·5	75·0
Sr	574	645	550	505	534	614	446	410	342	620	496	565	457
Y	18·0	15·6	17·6	17·0	22·0	20·0	19·8	16·2	13·6	11·0	7·6	13·8	11·0
Zr	114	123	125	155	190	183	146	145	194	65	92	111	110
Nb	5·5	6·7	6·1	7·2	8·0	8·3	9·5	9·3	9·2	7·5	7·5	8·3	7·8
Ba	620	745	675	772	763	915	1050	1150	1170	1000	1080	1250	1170
Th	3·5	5·2	4·3	5·3	9·1	7·5	11·2	7·8	13·7	–	9·9	8·0	9·0
La	17·4	18·0	18·0	22·0	36·5	29·0	32·0	28·0	32·00	28·30	21·0	43·0	26·00
Ce	33·0	35·0	36·5	37·0	59·0	45·0	60·0	44·0	59·00	55·00	39·0	89·0	49·00
Nd	19·5	18·4	20·0	23·0	36·0	28·0	28·0	24·5	21·50	25·00	19·5	43·5	20·50
Sm	4·30	4·10	4·20	4·50	7·40	6·20	5·60	–	3·70	–	4·10	8·00	3·60
Eu	1·13	1·14	1·21	1·25	1·66	1·49	1·14	1·05	0·80	1·07	1·13	1·55	0·90
Gd	4·10	3·45	4·25	4·05	5·10	4·60	4·55	–	3·00	–	2·80	5·25	2·70
Dy	3·15	3·00	3·30	3·25	4·35	3·85	3·55	2·92	2·20	2·13	1·70	3·00	1·96
Er	1·85	1·35	1·70	1·50	2·00	1·80	1·60	1·65	1·30	1·05	0·70	1·20	1·00
Yb	1·42	1·35	1·32	1·33	1·80	1·76	1·52	1·43	1·30	0·84	0·62	0·92	0·94
$^{87}Sr/^{86}Sr$	0·704310		0·704414			0·704415	0·704423	0·704460			0·704512	0·704543	
$^{143}Nd/^{144}Nd$	0·512743		0·512744			0·512640	0·512722	0·512726			0·512706	0·512617	

Edifice:	NCAY-MS								NCAY-SS					CLV		
Sample:	CAY168D	CAY169	CAY98	CAY8	CAY168A	CAY179A	CAY39	CAY87	CAY44A	CAY3B2	CAY2A	CAY3B1	CAY46B	CAY131A	CAY45C	LOD
SiO_2	58·00	60·85	61·30	61·90	63·65	65·20	66·50	67·00	58·90	60·30	62·40	64·30	65·00	66·00	58·90	
TiO_2	0·70	0·65	0·71	0·68	0·61	0·56	0·54	0·52	0·77	0·70	0·64	0·55	0·55	0·55	0·84	
Al_2O_3	16·50	16·05	16·20	17·00	16·10	15·90	16·15	15·50	17·10	17·20	17·10	16·20	16·60	15·80	14·95	
Fe_2O_3*	7·50	6·46	5·95	6·10	5·43	4·75	4·20	4·18	6·87	6·30	5·43	4·43	4·54	4·60	6·25	
MnO	0·11	0·10	0·09	0·08	0·08	0·07	0·06	0·06	0·10	0·10	0·09	0·07	0·08	0·08	0·10	
MgO	4·54	3·65	3·70	2·53	2·25	2·20	1·63	1·63	3·65	2·80	2·34	1·71	1·70	1·70	4·76	
CaO	6·65	6·26	5·95	5·30	4·72	4·23	3·67	3·84	6·35	5·80	4·91	4·15	4·20	4·35	6·50	
Na_2O	3·75	3·85	3·95	4·16	4·20	4·21	4·28	4·16	4·00	3·91	4·24	4·03	4·25	4·15	3·60	
K_2O	1·57	1·83	1·94	1·87	2·10	2·40	2·56	2·37	1·45	1·63	1·97	2·22	2·13	2·15	2·94	
P_2O_5	0·18	0·18	0·23	0·20	0·19	0·17	0·17	0·15	0·20	0·20	0·19	0·18	0·18	0·19	0·56	
LOI	−0·02	0·13	0·10	-0·18	0·30	0·13	0·01	0·62	0·53	0·72	0·15	1·58	0·47	0·57	0·14	
Total	99·48	100·01	100·12	99·64	99·63	99·82	99·77	100·03	99·92	99·66	99·46	99·42	99·70	100·14	99·54	
Sc	17·4	17·7	13·0	8·2	8·9	8·4	5·6	5·3	12·4	12·5	9·2	6·6	6·3	6·4	14·0	0·25
V	164	155	139	128	113	94	80	80	153	137	112	89	85	90	159	2·0
Cr	158	100	110	29	33	44	23	20	96	24	25	15	13	16	190	1·0
Co	24·0	21·0	22·0	17·0	14·0	16·0	12·0	10·0	23·0	19·0	15·0	13·0	11·5	14·0	22·0	1·0
Ni	51·0	26·0	48·0	16·0	18·0	19·0	12·5	12·0	37·0	14·0	13·0	9·0	8·0	10·0	41·0	2·0
Rb	35·5	51·0	50·0	51·0	57·5	72·0	69·0	66·0	35·0	43·0	51·0	63·0	58·0	63·0	96·0	1·0
Sr	534	515	675	565	528	555	560	540	600	565	570	542	555	532	1380	0·2
Y	12·1	12·4	11·1	9·3	10·7	8·3	7·9	7·0	11·7	12·4	11·2	9·4	10·1	10·0	17·0	0·5
Zr	90	110	101	105	110	117	56	65	114	89	90	73	77	82	211	1·0
Nb	4·6	5·9	7·5	5·8	6·4	6·5	7·5	8·1	5·8	5·7	6·2	6·7	6·6	7·0	8·0	0·8
Ba	630	800	950	736	890	980	985	980	625	675	811	933	900	1010	1480	2·0
Th	3·5	5·7	7·0	5·2	7·2	9·1	6·9	9·8	3·2	4·5	5·8	6·1	5·9	7·7	15·1	1·0
La	16·0	19·00	25·0	18·4	21·00	23·0	23·5	23·5	17·0	16·50	19·2	21·10	20·5	21·0	67·0	0·8
Ce	31·0	35·00	52·5	36·0	41·00	45·0	44·0	43·0	35·5	31·50	39·0	40·00	39·0	41·0	129·0	2·0
Nd	15·0	16·00	22·5	18·0	19·00	17·0	20·5	18·5	18·0	17·50	19·0	18·50	19·0	18·0	65·0	2·0
Sm	3·20	3·50	4·35	–	3·70	3·60	–	3·10	–	–	–	–	–	3·55	–	0·5
Eu	0·95	0·94	1·16	0·95	0·99	0·93	0·91	0·94	1·01	0·95	0·95	0·89	0·90	0·95	2·93	0·2
Gd	2·60	2·70	3·00	–	2·90	2·80	–	2·75	–	–	–	–	–	2·40	–	0·5
Dy	2·20	2·30	2·00	1·98	2·10	1·70	1·66	1·22	2·33	2·20	2·10	1·80	1·90	1·85	3·66	0·4
Er	1·10	1·20	1·00	0·85	1·00	0·75	0·70	0·55	1·20	1·20	1·20	0·90	0·90	0·90	1·50	0·8
Yb	0·94	1·07	0·84	0·62	0·79	0·70	0·56	0·41	0·92	1·05	0·90	0·73	0·78	0·76	1·07	0·2
$^{87}Sr/^{86}Sr$	0·704337		0·704324	0·704320		0·704452	0·704387	0·704428	0·704373				0·704418		0·704084	
$^{143}Nd/^{144}Nd$	0·512797		0·512802	0·512767		0·512684	0·512756	0·512744	0·512805				0·512771		0·512704	

Selected whole-rock analyses of CVC lavas: major element (wt %) and trace element (ppm) analyses were performed at the Université de Bretagne Occidentale, Brest (France), by ICP−AES, except Rb, performed by AES. See Cotten *et al.* (1995) for the methods. Relative standard deviations (3σ) are ≤2% and 5% for major and trace elements, respectively. LOD, limit of detection (in ppm); LOI, loss on ignition. Isotope ratios were determined at the Laboratoire Magmas et Volcans of the Université Blaise Pascal, Clermont-Ferrand (France). $^{86}Sr/^{88}Sr$ is corrected for mass fractionation by normalizing to $^{87}Sr/^{86}Sr = 0{\cdot}1194$ and given relative to NBS SRM987 standard value of 0·710262 ($n = 4$). $^{143}Nd/^{144}Nd$ is corrected for mass fractionation by normalizing to $^{146}Nd/^{144}Nd = 0{\cdot}7219$ and given relative to La Jolla Nd standard value of 0·511960 ($n = 4$). *Total iron as Fe_2O_3.

Table 7: Geochemical characteristic of adakites compared with range of variation in CVC rocks

	Adakites	VCAY	NCAY-ANG	NCAY-MS	NCAY-SS	CLV
SiO_2 wt %	>56	57·3–72·8 (62·2)	63·6–68·6 (66·0)	58·3–67·4 (63·5)	57·6–66·4 (63·0)	59·3–59·9 (59·6)
Al_2O_3 wt %	>15	15·0–18·6 (17·0)	15·3–17·6 (16·5)	15·6–17·3 (16·4)	15·9–18·0 (16·8)	15·0–15·5 (15·2)
Na_2O wt %	3·5–7·5	3·1–4·5 (3·9)	3·6–4·5 (4·1)	3·8–4·6 (4·1)	3·9–4·6 (4·2)	3·6–3·7 (3·7)
K_2O/Na_2O	<0·5	0·4–0·9 (0·6)	0·5–0·7 (0·6)	0·4–0·7 (0·5)	0·3–0·6 (0·4)	0·8 (0·8)
Sr ppm	>400–600	342–656 (538)	441–625 (535)	490–675 (566)	518–644 (569)	1250–1380 (1324)
Y ppm	<18	13·6–27·0 (18·1)	7·6–19·0 (11·7)	7·0–12·4 (9·7)	8·9–19·0 (11·2)	16·2–17·0 (16·8)
Yb ppm	<1·9	1·3–2·5 (1·5)	0·6–1·5 (0·9)	0·4–1·1 (0·8)	0·7–1·4 (0·9)	1·0–1·1 (1·1)
Sr/Y	>40	18–41 (30)	24–70 (49)	42–79 (59)	32–63 (52)	77–81 (79)
La/Yb	>20	10–25 (17)	19–47 (33)	17–57 (29)	10–33 (22)	59–63 (61)
$^{87}Sr/^{86}Sr$	<0·7045	0·7043–0·7045	0·7045	0·7044	0·7043–0·7045	0·7041
$^{143}Nd/^{144}Nd$	>0·5129	0·5126–0·5127	0·5127	0·5128	0·5126–0·5128	0·5127

After Defant & Drummond (1990), Maury *et al*. (1996) and Martin (1999). Averages are given in parentheses.

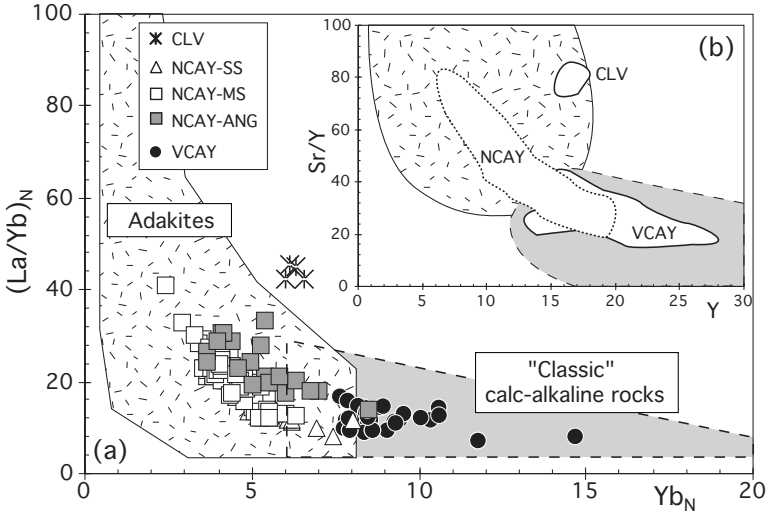

Fig. 8. Discrimination diagrams for calc-alkaline and adakitic series. (a) $(La/Yb)_N$ vs Yb_N diagram (Martin, 1999). (b) Sr/Y vs Y diagram (Drummond & Defant, 1990).

Isotopic data

The Sr and Nd isotopic ratios of both edifices are identical ($^{87}Sr/^{86}Sr$: 0·704310–0·704543; $^{143}Nd/^{144}Nd$: 0·512617–0·512805; Fig. 9; Table 6). All (but one) of the samples define a negative correlation in a $^{143}Nd/^{144}Nd$ vs $^{87}Sr/^{86}Sr$ diagram. The only sample plotting out of this trend is a CLV andesite ($^{87}Sr/^{86}Sr$: 0·704084; $^{143}Nd/^{144}Nd$: 0·512704) with an apparently lower $^{87}Sr/^{86}Sr$ value than for other CVC rocks. However, all samples are typical of the NVZ (Bourdon *et al*., 2003), which is characterized by a large variation in $^{143}Nd/^{144}Nd$, with a weak variation in $^{87}Sr/^{86}Sr$ (Fig. 9a). CVC data partially overlap the field of Eastern Cordillera volcanic rocks and extend this field towards higher $^{87}Sr/^{86}Sr$ and lower $^{143}Nd/^{144}Nd$ values (Fig. 9b).

Figure 9a shows that CVC rocks plot transverse to the extension of the trend defined by MORB and OIB of the East Pacific Rise, Galápagos Spreading Centre, and the Galápagos hotspot (White *et al*., 1993 and references therein). Figure 9a also shows the field for the Western Cordillera basement, lower crustal xenoliths from southwestern Colombia, and the crustal Eastern Cordillera basement. The relatively unradiogenic Sr-isotopic composition of the CVC rocks precludes significant assimilation of western Cordillera basement rocks. On the contrary, the field of lower crustal xenoliths overlaps the isotopic data for Cayambe (and all other NVZ volcanoes), indicating that assimilation of such material by NVZ magmas may have occurred. The Ecuadorian Nd–Sr isotopic

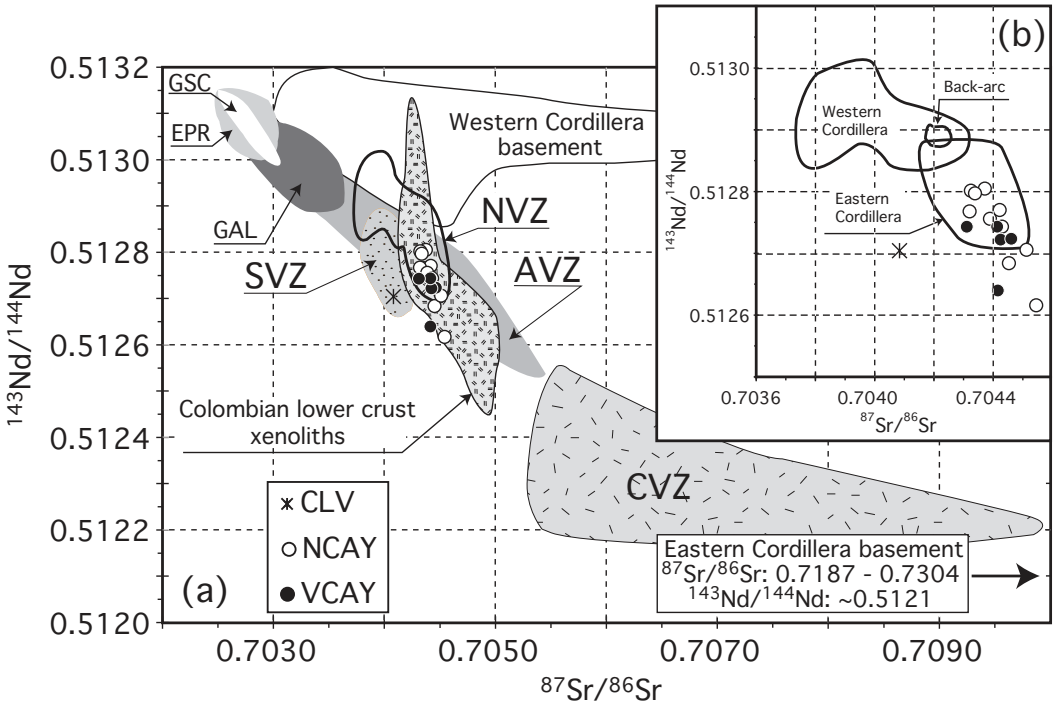

Fig. 9. (a) $^{143}Nd/^{144}Nd$ vs $^{87}Sr/^{86}Sr$ diagram for CVC rocks, compared with published isotopic data for the NVZ (Bourdon *et al.*, 2003). Fields of isotopic data for the Galápagos Spreading Centre (GSC), East Pacific Rise (EPR) and Galápagos Islands (GAL) from White *et al.* (1993) and references therein. Field for Central Volcanic Zone (CVZ), Southern Volcanic Zone (SVZ) and Austral Volcanic Zone (AVZ) from Stern *et al.* (1984), Wilson (1989), Davidson *et al.* (1990) and Stern & Kilian (1996). Data for isotopic variation of upper crust basement from Litherland *et al.* (1994), Kilian *et al.* (1995) and Reynaud *et al.* (1999). Isotopic composition of lower crust xenoliths from Weber *et al.* (2002). (b) Detailed $^{143}Nd/^{144}Nd$ vs $^{87}Sr/^{86}Sr$ diagram showing the CVC data compared with data from Western Cordillera and Eastern Cordillera volcanic rocks.

data partially overlap the SVZ and AVZ fields (Stern *et al.*, 1984; Stern & Kilian, 1996), but are clearly less radiogenic in Sr than the CVZ lavas, for which crustal assimilation of ancient crust is important (Davidson *et al.*, 1990).

PETROGENESIS OF CAYAMBE VOLCANIC ROCKS

Mineral–liquid equilibrium and magma mixing

Figure 10 indicates the *mg*-number of liquids in equilibrium with pyroxenes (clinopyroxene and orthopyroxene) versus the *mg*-number of their host rocks. The *mg*-numbers of the theoretical liquids have been calculated using the composition of phenocryst minerals and mineral–liquid partition coefficients (K_D). Typical $K_D^{Fe^{2+}/Mg}$ are 0·25 (0·2–0·4, maximum–minimum range) for clinopyroxene and 0·3 (0·2–0·4) for orthopyroxene (Grove *et al.*, 1997; Gaetani & Grove, 1998). Because the host rocks represent mixtures of phenocrysts and liquids, a shift to a higher *mg*-number of the host rock indicates phenocryst accumulation. In contrast, bulk-rock *mg*-numbers less than predicted (grey field in Fig. 10) indicate that the phenocryst minerals cannot have crystallized from a magma having the same composition as their host rock. All VCAY compositions are low in MgO, compared with those from the NCAY and CLV edifices. Scattering could be explained by: (1) variation in K_D values, which depends on pressure, temperature and magma composition (Ulmer, 1989; Straub & Martin-del-Pozzo, 2001); or, more likely, (2) crystallization of the phenocrysts from a magma whose composition differs from that of the host rock (Heath *et al.*, 1998).

In summary, magma mixing in the CVC petrogenesis is supported by:

(1) disequilibrium between pyroxene phenocryst compositions and host andesitic lavas in VCAY;
(2) macroscopic mingling and mixing textures in NCAY-MS and NCAY-SS rocks;
(3) large plagioclase compositional ranges, with reverse and complex zoning, especially in heterogeneous samples belonging to the younger edifice;
(4) two populations of amphibole in dacitic rock of NCAY;
(5) reverse zoning of pyroxenes in NCAY lavas, and Mg-rich orthopyroxene, clinopyroxene and olivine phenocrysts in NCAY dacites;

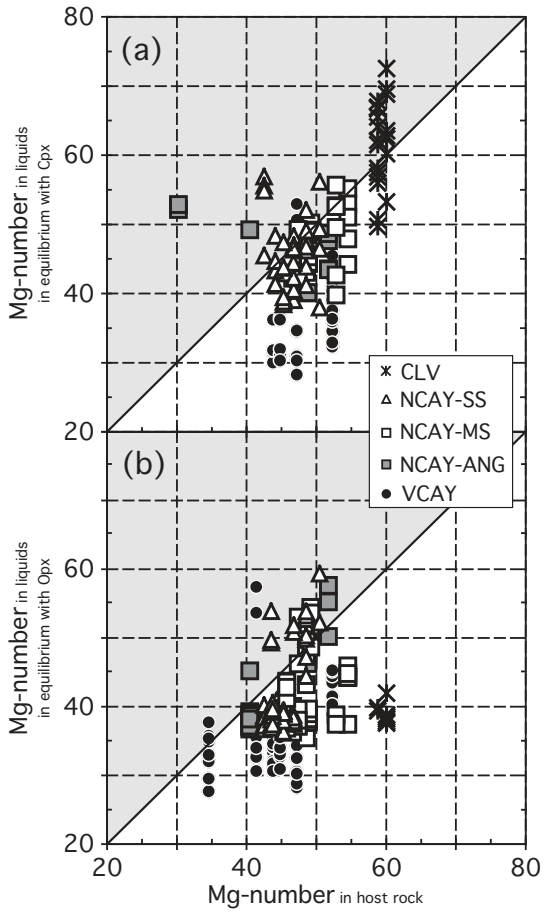

Fig. 10. Plot of theoretical *mg*-number of liquids in equilibrium with clinopyroxene (a) and orthopyroxene (b) vs *mg*-number of their host rocks. The theoretical *mg*-number of the liquids was calculated using K_D values from the literature (Gaetani *et al.*, 1993; Grove *et al.*, 1997) and the observed composition of pyroxenes in the lavas. The grey fields correspond to host rocks with composition too low in magnesium to be in equilibrium with their Mg-rich pyroxenes.

(6) the presence of Mg-poor and Mg-rich orthopyroxene and clinopyroxene in the same NCAY lavas;
(7) the presence in some NCAY-MS and NCAY-SS rocks of high-Al_2O_3 pyroxenes;
(8) the strongly linear correlations in Harker diagrams for NCAY-SS rock compositions.

Fractional crystallization in VCAY and NCAY lavas

Normally zoned minerals, as well as different fractionating phases in each series, indicate that fractional crystallization could have occurred during the petrogenesis of CVC rocks. In the VCAY edifice, fractionation of observed phases (Pl + Cpx + Opx + Mag) does not, however, account for the trace element variations. For example, elements usually positively correlated with silica (HFSE, HREE; Fig. 7) remain constant with increasing silica (or another differentiation index, e.g. Rb), and trace element ratios (e.g. La/Yb, La/Sm, Th/Y; Fig. 11) exhibit significant variations, which cannot be explained by fractionation of observed minerals. Likewise, VCAY dacites cannot be derived from andesites by simple fractional crystallization, because the dacites have higher contents of Mg, Ni and Cr than the andesites (Fig. 7).

In the NCAY suite, fractionation of an amphibole-rich assemblage (Pl + Amph + Mag ± Cpx ± Opx) could explain the HREE depletion of these magmas and their *pseudo*-adakitic signature (see Castillo *et al.*, 1999). However, in intermediate and felsic magmas, amphibole fractionation produces depletion in both MREE (e.g. Sm) and HREE (e.g. Yb), resulting in high La/Yb and La/Sm but almost constant Sm/Yb values. This is not the case for the NCAY rocks, which have wide variations in trace element ratios (Fig. 11). Particularly, NCAY magmas display La/Yb and Sm/Yb variations, pointing to garnet involvement in their petrogenesis.

Crustal assimilation

Assimilation of crustal material, especially during the petrogenesis of the NCAY rocks, is supported by good correlations between Nd–Sr isotopic ratios and SiO_2, Th, Rb, La and other trace element ratios (e.g. Rb/Sr; Fig. 12). In order to test this hypothesis, an AFC model (DePaolo, 1981) has been applied, assuming an andesitic parental magma (CAY44B) and two potential crustal contaminants: (1) a granite representative of highly radiogenic upper crust (the Tres Lagunas granite; $^{87}Sr/^{86}Sr$: 0·7187–0·7304 and $^{143}Nd/^{144}Nd$: ~0·5121; Litherland *et al.*, 1994); and (2) an amphibolite xenolith from Colombia ($^{87}Sr/^{86}Sr$: 0·70412–0·70495 and $^{143}Nd/^{144}Nd$: 0·51309–0·51245; Weber *et al.*, 2002). Calculations account for the Nd–Sr isotopic and some trace element characteristics of the NCAY rocks (Fig. 12), with two distinct degrees of assimilation, according to the choice of contaminant. In one model, the isotopic data are reproduced by an upper crustal AFC process with variable assimilation/crystallization rates ($r \sim 0{\cdot}05$–$0{\cdot}4$). This model suggests small amounts of assimilation of high $^{87}Sr/^{86}Sr$ granite (*c.* 3–13%)—an estimate similar to that calculated by Bourdon *et al.* (2002*b*) for Antisana volcano. On the other hand, assimilation of lower basaltic crust (amphibolite) by AFC processes requires larger degrees of assimilation (*c.* 10–30%; $r \sim 0{\cdot}2$–$0{\cdot}6$), which approach the estimation of Hammersley & DePaolo (2002) for Chalupas caldera.

In summary, crustal assimilation reproduces trace element enrichments (e.g. Rb and La), but depletion in HREE and Y (one aspect of the adakitic signature of CVC magmas) is not explained by AFC models. Finally, the lack of isotopic contrast between the VCAY and NCAY lavas indicates that the differences in mineral

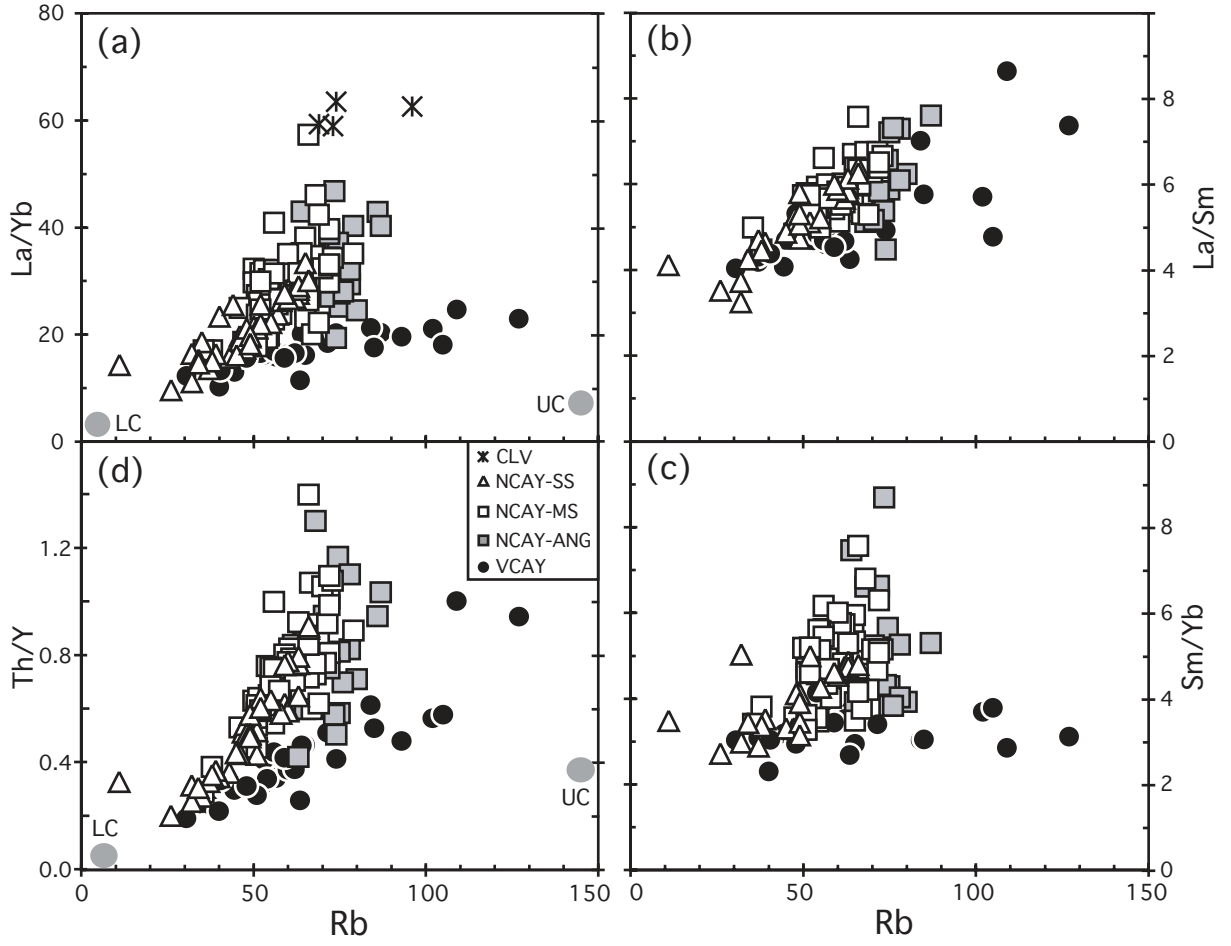

Fig. 11. Trace element ratios vs Rb used as a differentiation index. (a) La/Yb; (b) La/Sm; (c) Sm/Yb and (d) Th/Y. Upper crustal (UC) and lower crustal (LC) compositions are indicated in (a) and (d) (Litherland *et al.*, 1994; Weber *et al.*, 2002).

assemblage and major and trace element chemistry cannot be explained by different degrees or type of crustal contamination.

The origin of the adakitic component: lower crust melting versus slab melting

In an overview of Quaternary NVZ magmatism, Monzier *et al.* (2003) pointed out the high MgO, Ni and Cr (and, to a lesser extent, Na_2O) contents of the lavas and their strong depletion in Y and HREE. Moreover, Nb contents show a wide and systematic range of variation from low-Nb volcanic front lavas to mid- to high-Nb rocks in the main arc (e.g. Cayambe volcanic complex) and very high Nb contents in back-arc volcanic rocks (see also Barragán *et al.*, 1998; Bourdon *et al.*, 2003). In addition to these across-arc variations, lavas from the volcanic front display the strongest adakitic characteristics, as well as the lowest $^{87}Sr/^{86}Sr$ and highest $^{143}Nd/^{144}Nd$ ratios, whereas volcanic rocks from the main arc have more 'classic' calc-alkaline signatures (with the exception of the Nevado Cayambe volcano) and higher $^{87}Sr/^{86}Sr$ and lower $^{143}Nd/^{144}Nd$. Thus, Nd–Sr isotopic variations across the Ecuadorian arc may suggest either an increase of crustal involvement in arc magma genesis from west to east, or, more likely, a different isotopic composition between the younger, less evolved crust below the Western Cordillera and the older, more siliceous crust under the Eastern Cordillera.

Adakites are believed to form by melting of a basaltic, MORB-like source, leaving an eclogitic or garnet-bearing amphibolitic residue (Defant & Drummond, 1990; Martin, 1999). The geological and geodynamic setting of the Ecuadorian arc is consistent with either the melting of the lower crust (whether formed by accretion of mafic terranes or by basalt underplating; Kilian *et al.*, 1995; Monzier *et al.*, 1997; Arculus *et al.*, 1999) or slab melting (Samaniego, 2001; Bourdon *et al.*, 2002*a*, 2002*b*, 2003). In either case, experimental studies imply that adakitic magmas can only be produced if the basaltic source is water-rich, and at a sufficient depth to allow garnet

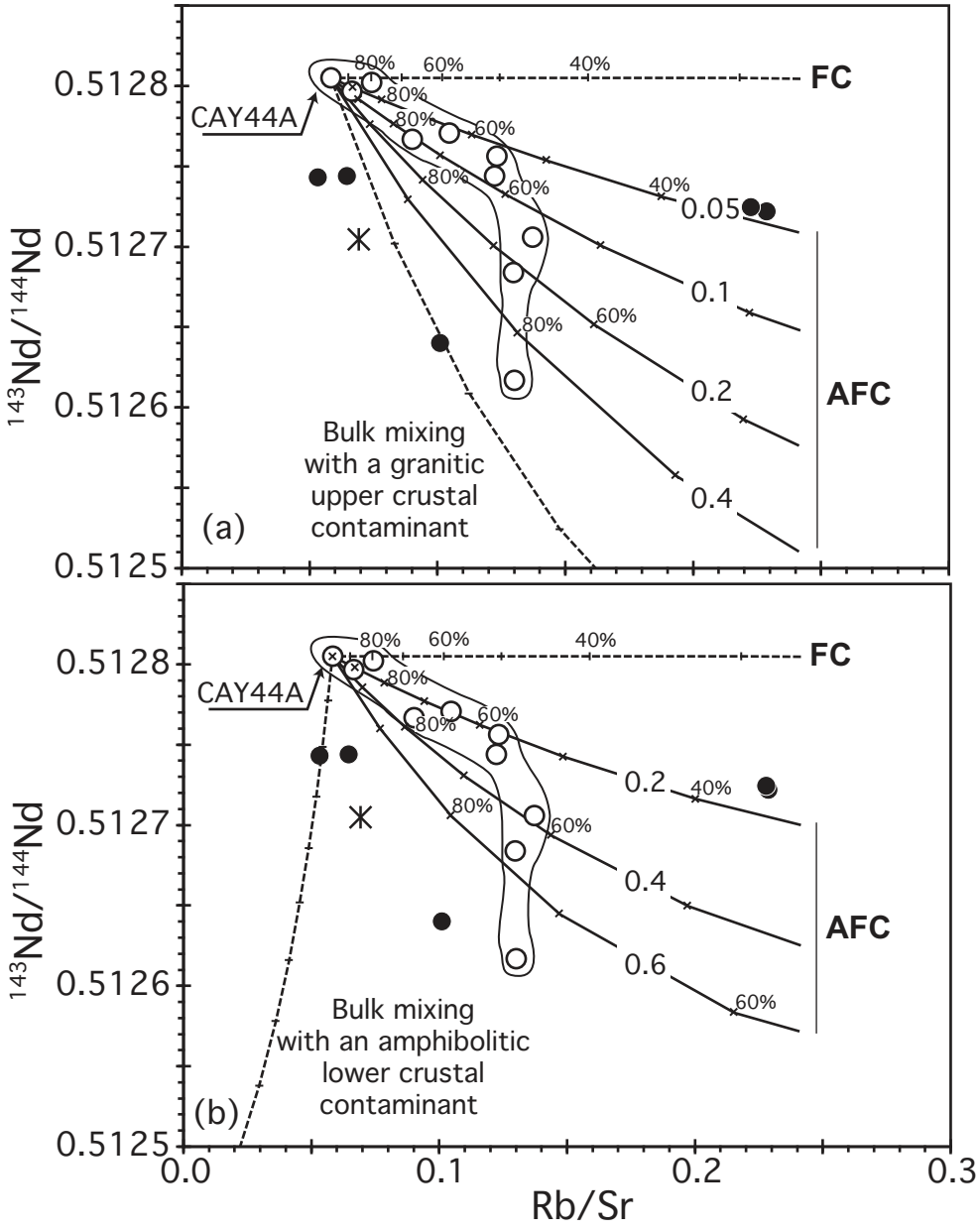

Fig. 12. $^{143}Nd/^{144}Nd$ vs Rb/Sr showing AFC models (continuous lines) for different *r* values (ratio of mass assimilated to mass fractionated). Each tick mark on the AFC and FC model curves corresponds to the fraction of magma remaining. (a) Granitic upper crustal contaminant; (b) amphibolitic lower crustal contaminant. CAY44A is a primitive rock from the NCAY series. Trends for simple fractional crystallization and bulk mixing are also shown (dashed lines). (See text for details).

stability (Rapp *et al.*, 1991; Sen & Dunn, 1994; Rapp & Watson, 1995; Prouteau *et al.*, 1999). In addition, Prouteau *et al.* (2001) proposed that because free water is available in the subducted slab, fluid-present melting reactions occur there and generate siliceous, trondhjemitic melts. This requirement supports an origin of adakitic magmas in the subducted slab, where excess water would be supplied by dehydration of hydrous phases from the slab (Schmidt & Poli, 1998) or serpentine breakdown in the mantle underlying the oceanic crust (Ulmer & Trommsdorff, 1995). In addition, the MgO, Ni and Cr contents of adakites are higher than those of liquids produced by experimental melting of basalts. Such enrichments would reflect interactions between the slab-derived adakitic liquids and peridotite during their ascent through the mantle wedge (Rapp *et al.*, 1999; Smithies, 2000; Prouteau *et al.*, 2001; Martin & Moyen, 2002).

Partial melting of garnetiferous lower crust is an alternative way to explain adakitic magmatism in a tectonically thickened continental crust. Melting of the lower crust occurs through delamination (Kay & Kay, 1993) or basaltic underplating (Atherton & Petford, 1993; Annen & Sparks, 2002). Lower crust melting via delamination produces crustal uplift and extension, changes in stress regime and variations in mantle-derived magmatism. No evidence for any of these processes is found in the Ecuadorian Andes. In addition, Weber *et al.* (2002), on the basis of petrological data on crustal xenoliths from southwestern Colombia, concluded that the lower crust in this part of the NVZ was formed by 'lateral crustal growth, involving subduction–accretion of heterogeneous material from the subducting slab', contending that limited vertical accretion occurred (i.e. underplating).

On the contrary, beneath the CVC, the lack of seismic events deeper than 100 km could be considered as reflecting an anomalously hot slab (see Stern, 2002), which, in turn, may favour its partial melting. Also, the Mg- and Nb-rich compositions of the Ecuadorian magmas imply interactions between the adakitic magmas and mantle peridotite, that obviously argue in favour of an origin of adakites through melting of a subducted slab rather than of lower crustal rocks. The higher geothermal gradients along the Wadati–Benioff zone needed to explain slab partial melting can be related to the presence of the Carnegie Ridge under the volcanic arc (Gutscher *et al.*, 1999). The effect of ridge subduction would be to increase the rate of shear heating and to increase the geothermal gradient along the subduction plane (Peacock *et al.*, 1994). Slab melting has been tested for the adakitic-like rocks of the NCAY series. Mass-balance calculations based on major element abundances (Bryan *et al.*, 1969) provide an estimation of the mineralogical composition of the residue, which is presumed to be eclogitic. Theoretical trace-element abundances were computed using a batch partial melting model (Shaw, 1970), for an E-MORB source (Sun & McDonough, 1989), considered representative of the Carnegie Ridge basalts. The computed slab melt compositions are not in perfect agreement with NCAY compositions (see below, curve 4 in Fig. 14a, and Fig. 14b), thus indicating that this simple model is inadequate.

Mantle participation and petrogenetic model

Interactions between slab melts and mantle peridotite can occur by: (1) metasomatism of the mantle wedge by slab melts, followed by remelting of the metasomatized mantle peridotite (Schiano *et al.*, 1995; Yogodzinski *et al.*, 1995; Rapp *et al.*, 1999; Prouteau *et al.*, 2001); (2) contamination of adakitic melts by peridotite during their ascent through the mantle wedge, as proposed for the adakites of Austral Volcanic Zone of the Andes (Stern & Kilian, 1996); and (3) mixing between adakitic magmas and mantle-derived magmas, as envisaged for Aleutian adakites (Yogodzinski & Kelemen, 1998).

Enrichment of the peridotitic source can be estimated using the composition of the most primitive lavas normalized to N-MORB (Pearce & Parkinson, 1993). HFSE and HREE (Nb, Zr, Ti, Y and Yb) have $K_D^{\text{mineral/fluid}} \gg 1$ and are not mobilized by aqueous fluids (Keppler, 1996). Thus, curves connecting these elements (e.g. the Nb–Yb curve, Fig. 13) should represent the mantle composition prior to metasomatism by slab-derived fluids. In this figure, the most primitive CVC rocks display a negative slope as a result of lower degrees of melting (Barragán *et al.*, 1998). Moreover, compared with N-MORB, values of >1 (especially for Nb) point to mantle enrichment that could be related to an OIB component (Stern & Ito, 1983) or to a slab-derived metasomatic agent different from aqueous fluids (Ringwood, 1974). On the basis of the trace element and isotope characteristics of the lavas, participation of an OIB-type component has been excluded for other Ecuadorian volcanoes: Antisana Eastern Cordillera) and Sumaco (back-arc) (Barragán *et al.*, 1998; Bourdon *et al.*, 2003). Conversely, the hypothesis of an adakitic metasomatism is supported by the Nb enrichment of Eastern Cordillera and back-arc volcanic rocks, given that slab-derived melts are able to transfer Nb from the slab into the mantle wedge (Defant & Drummond, 1990; Maury *et al.*, 1996; Sajona *et al.*, 1996).

In addition, HREE and Y have MORB-normalized values lower than 1, and NCAY andesite (CAY168D) is poorer in HREE than VCAY (CAY56) and CLV (CAY45C) andesites. Because garnet is the only phase able to incorporate large amounts of HREE under upper mantle conditions ($K_{\text{DHREE}}^{\text{garnet/liquid}} > 1$), depletion of these elements in a magma reflects a garnet-bearing mantle source.

Melting of a garnet-bearing mantle source enriched by slab melts (adakite–metasomatized mantle—AMM) is modelled in Fig. 14a. First, the composition of this AMM has been calculated using a bulk mixing process (Fig. 14c) between a depleted mantle (97%) and an adakitic magma (3%). Both lherzolitic (Ol + Cpx + Opx) and garnet-bearing lherzolitic (Ol + Cpx + Opx + Grt) residues can account for the origin of CVC andesites (curves 1, 2 and 3 in Fig. 14a; Fig. 14d and e). However, NCAY andesites are accounted for only when garnet is a residual phase. Residual garnet during peridotite melting in arc settings requires at least two conditions: (1) a depth of >75 km (Tatsumi & Eggins, 1995) and (2) low degree of melting (<15%), as garnet is one of the first phases consumed by melting (Pearce & Parkinson, 1993). Experiments on siliceous melt–peridotite interactions

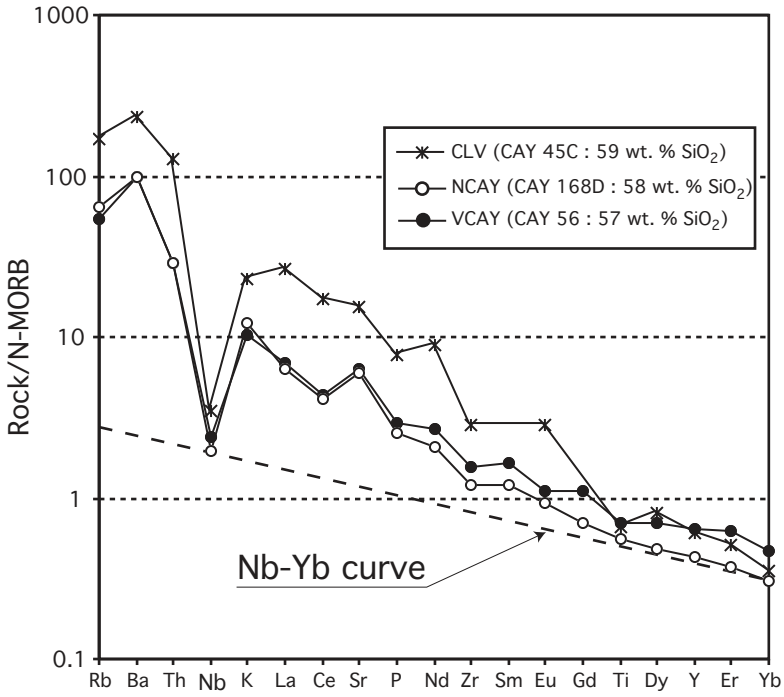

Fig. 13. MORB-normalized multi-element diagram (N-MORB values from Pearce & Parkinson, 1993) for primitive rocks of the CVC. Nb–Yb line for CAY 168 andesite from the NCAY edifice is indicated by the dashed line.

show that the resulting metasomatized peridotite consists of pyroxene + garnet + amphibole + phlogopite (Carroll & Wyllie, 1989; Sen & Dunn, 1995; Rapp *et al.*, 1999; Prouteau *et al.*, 2001). During subsequent melting of this assemblage, amphibole melts first, producing garnet and clinopyroxene in a ratio of 3:1 (Francis & Ludden, 1995; Dalpé & Baker, 2000; Calmus *et al.*, 2003). In this case, garnet is stable over degrees of melting sufficiently great to generate HREE-depleted magmas. Figure 14 shows that the genesis of the primitive andesites of the CVC can be explained by the partial melting of a mantle peridotite metasomatized by slab melts, and leave a garnet-bearing residue. However, this process (and subsequent fractional crystallization and crustal assimilation) cannot account for the genesis of all the lavas, and especially of the NCAY dacites. In the previous discussion, we demonstrated that these dacites are not pure slab melts (curve 4 in Fig. 14a, and Fig. 14b). In the same figure, the composition of liquids generated by the mixing between pure slab melt (ADK) and metasomatized mantle melts are shown (curve 5 in Fig. 14a). The mixing hypothesis is consistent with field observations and mineralogical evidence for magma mixing being important in the genesis of the NCAY dacites. Therefore, mixing between adakitic and andesitic end-members explains best most of the chemical characteristics of the NCAY and the dacitic compositions from the VCAY edifice which are not explained by fractional crystallization processes (curve 6 in Fig. 14a).

CONCLUSION: TEMPORAL EVOLUTION OF MAGMATISM

In the Cayambe area, Pleistocene magmatism is characterized by the evolution from an old, mostly effusive volcano (VCAY) to young explosive edifices, which constitute the NCAY. Volcanic activity that led to construction of VCAY initiated before 1·1 Ma and ended around 1·0 Ma. After a period of quiescence of some 0·6 Myr, marked by an important erosive discordance, volcanic activity resumed with NCAY-ANG construction at *c.* 0·4 Ma, but the most important activity developed during the last 250 kyr (NCAY-MS and NCAY-SS edifices).

The volcanic evolution is accompanied by a drastic decrease of Y with time (and HREE) (from 14–27 ppm for VCAY to 7–19 ppm for NCAY), accompanied by a weak but significant decrease in incompatible element concentrations. These geochemical differences, and the ubiquitous presence of amphibole in the NCAY lavas, reflect the transition from calc-alkaline to adakite-like magmatism in this part of the arc.

Fractional crystallization is unable to explain the diversity of both series and also the evolution from VCAY to NCAY magmas. Assimilation of crustal rocks is needed to explain the Nd–Sr isotopic signature of the Cayambe rocks, but trace element concentrations and ratios preclude assimilation and crystallization from being the principal mechanism relating the different magmas.

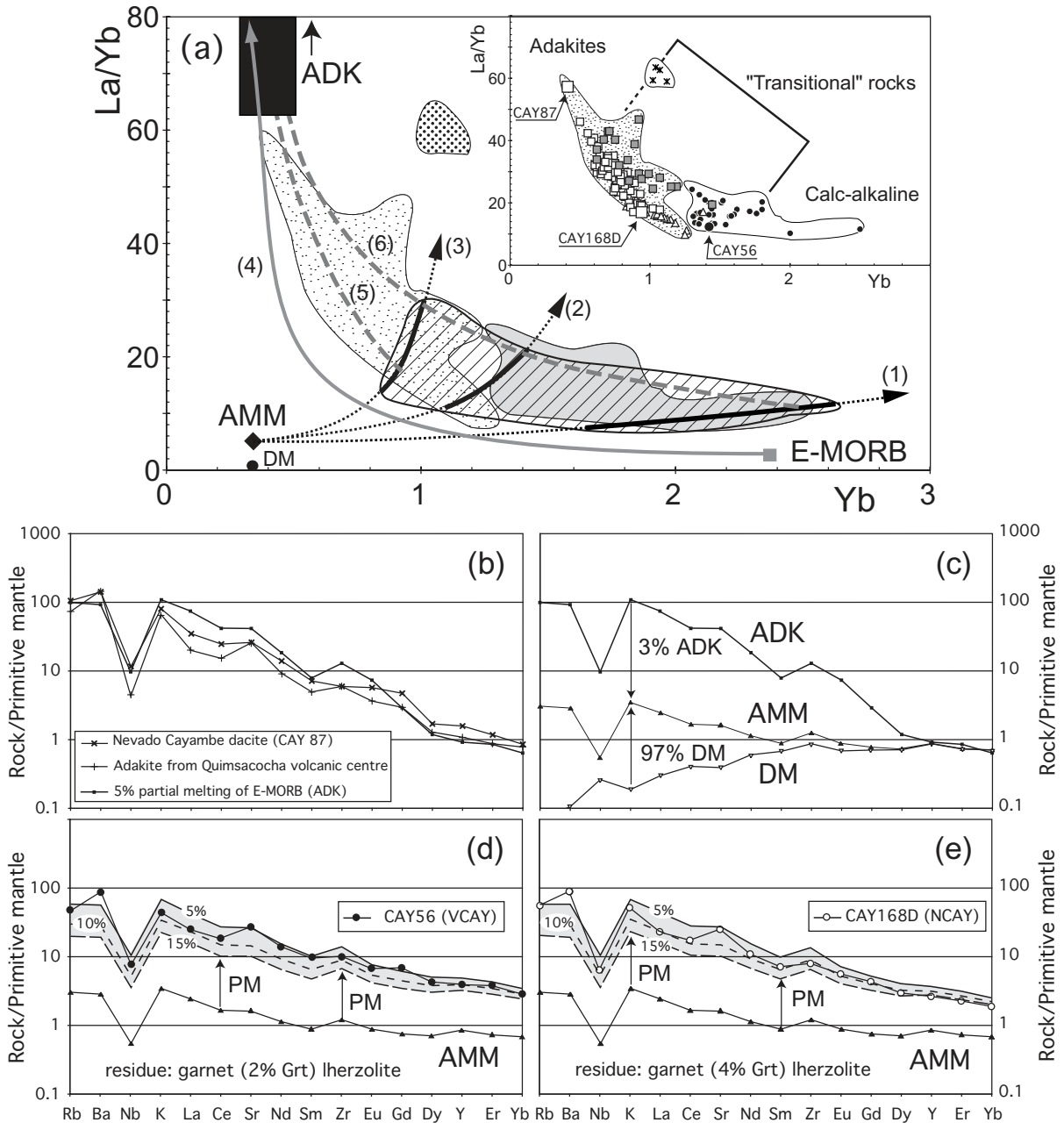

Fig. 14. Petrogenetic model for the CVC magmas. (a) La/Yb vs Yb diagram showing fields for the NCAY, VCAY and CLV edifices. Batch partial melting models (Shaw, 1970) for an adakite-metasomatized mantle (AMM) are indicated by numbers in parentheses. Three residual modal compositions are considered: (curve 1) lherzolitic (0% Grt) residue (69% Ol + 11% Cpx + 20% Opx); (curve 2) garnet lherzolitic (2% Grt) residue (61% Ol + 12% Cpx + 25% Opx + 2% Grt); (curve 3) garnet lherzolitic (4% Grt) residue (61% Ol + 12% Cpx + 23% Opx + 4% Grt). Bold parts of these curves represents degrees of melting ranging from 5 to 15%. Ruled field is the domain of magma composition obtained by AMM melting. Slab partial melting of an enriched (E-MORB) basaltic source (curve 4), leaving an eclogitic residue (61% Cpx + 38% Grt + 1% Rt). Two bulk-mixing models are also shown: (curve 5) between an adakitic (ADK) and an andesitic (adakitic-like) pole; and (curve 6) between an adakitic (ADK) and a calc-alkaline end-member. Partition coefficients used for mantle melting (mafic liquids) were given by Halliday *et al.* (1995); and those for slab-melting models (acid and/or intermediate liquids) given by Martin (1987). Inset: La/Yb vs Yb diagram showing analytical data for CVC lavas. Same symbols as for Fig. 7. Lavas whose compositions could be explained by melting of an AMM source (referred to as transitional or adakite-like rocks) are located between true adakites and calc-alkaline volcanic rocks. (b) Multi-element diagram normalized to primitive mantle showing a 5% partial melting of an enriched basaltic source (E-MORB, Sun & McDonough, 1989) leaving an eclogitic residue (ADK, same model as curve 4). An adakite from Quimsacocha volcanic centre (Beate *et al.*, 2001) and a dacite from Nevado Cayambe volcano (CAY87) are also shown for comparison. (c) Mantle metasomatism by an adakitic magma is modelled by mass-balance. Adakite-metasomatized mantle (AMM) results from 97% depleted mantle (Yogodzinski *et al.*, 1995) and 3% of an adakitic component (resulting from a 5% partial melt of an E-MORB source). (d) Batch partial melting of an AMM source leaving a garnet lherzolitic (2% Grt) residue (same model as curve 2). A primitive andesite of the VCAY edifice (CAY56) results from 5–15% partial melting of such a source. (e) Batch partial melting of an AMM source leaving a garnet lherzolitic (4% Grt) residue (same model as curve 3). A primitive andesite of the NCAY edifice (CAY168D) results from 5–15% partial melting of such a source. PM, partial melting.

The source of the VCAY magmas is an enriched mantle source metasomatized by slab-derived melts. Partial melting of such a source, leaving a garnet-bearing residue, accounts for the genesis of the NCAY andesites, whereas mixing between adakitic magmas and mantle melts generates the NCAY dacites. During the VCAY construction, slab melts were consumed in reactions with peridotite, which produced the AMM enriched mantle that subsequently remelted. During NCAY activity, melts derived from the mantle wedge mixed with primary adakite magma, resulting in increasingly adakitic signatures with time. This evolution is probably a result of the arrival of the Carnegie Ridge at the subduction zone, which modified the geothermal gradient along the Wadati–Benioff zone, favouring slab partial melting.

ACKNOWLEDGEMENTS

We thank C. Bosq for carrying out the isotopic analyses and E. Bourdon for providing one additional isotopic analysis. Stimulating discussions with E. Bourdon and J.-L. Le Pennec were much appreciated. Constructive reviews by R. Conrey and an anonymous referee greatly helped to improve the manuscript. We deeply thank Dennis Geist for editorial handling and help with the final revision of the manuscript. This work is part of P.S.'s Ph.D. financed by the Ecuadorian 'Fundación para la Ciencia y la Tecnología' (FUNDACYT), the French 'Institut de Recherche pour le Développement' (IRD) and the Escuela Politécnica Nacional (EPN) of Quito (Ecuador). Contribution UMR Géosciences Azur No. 705.

SUPPLEMENTARY DATA

Supplementary data for this paper are available at *Journal of Petrology* online.

REFERENCES

Abratis, M. & Wörner, G. (2001). Ridge collision, slab-window formation, and flux of Pacific asthenosphere into the Caribbean realm. *Geology* **29**, 127–130.

Annen, C. & Sparks, R. S. J. (2002). Effects of repetitive emplacement of basaltic intrusions on thermal evolution and melt generation in the crust. *Earth and Planetary Science Letters* **203**, 937–955.

Arculus, R. J., Lapierre, H. & Jaillard, E. (1999). Geochemical window into subduction and accretion processes: Raspas metamorphic complex, Ecuador. *Geology* **27**, 547–550.

Atherton, M. P. & Petford, N. (1993). Generation of sodium-rich magmas from newly underplated basaltic crust. *Nature* **362**, 144–146.

Barragán, R., Geist, D., Hall, M. L., Larson, P. & Kurz, M. (1998). Subduction controls on the compositions of lavas from the Ecuadorian Andes. *Earth and Planetary Science Letters* **154**, 153–166.

Beate, B., Monzier, M., Spikings, R., Cotten, J., Silva, J., Bourdon, E. & Eissen, J.-P. (2001). Mio-Pliocene adakite generation related to flat subduction in Southern Ecuador: the Quimsacocha volcanic center. *Earth and Planetary Science Letters* **192**, 561–570.

Bourdon, E., Eissen, J.-P., Gutscher, M.-A., Monzier, M., Samaniego, P., Robin, C., Bollinger, C. & Cotten, J. (2002*a*). Slab melting and slab melt metasomatism in the Northern Andean Volcanic Zone: adakites and high-Mg andesites from Pichincha volcano (Ecuador). *Bulletin de la Societé Géologique de France* **173**, 195–206.

Bourdon, E., Eissen, J.-P., Monzier, M., Robin, C., Martin, H., Cotten, J. & Hall, M. L. (2002*b*). Adakite-like lavas from Antisana Volcano (Ecuador): evidence for slab melt metasomatism beneath the Andean Northern Volcanic Zone. *Journal of Petrology* **43**, 199–217.

Bourdon, E., Eissen, J.-P., Gutscher, M.-A., Monzier, M., Hall, M. L. & Cotten, J. (2003). Magmatic response to early aseismic ridge subduction: the Ecuadorian margin case (South America). *Earth and Planetary Science Letters* **205**, 123–138.

Bryan, W. B., Finger, L. W. & Chayes, F. (1969). Estimating proportions in petrographic mixing equations by least-squares approximation. *Science* **163**, 926–927.

Calmus, T., Aguillón-Robles, A., Maury, R. C., Bellon, H., Benoit, M., Cotten, J., Bourgois, J. & Michaud, F. (2003). Spatial and temporal evolution of basalts and magnesian andesites ('bajaites') from Baja California, Mexico: the role of slab melts. *Lithos* **66**, 77–105.

Carroll, M. R. & Wyllie, P. J. (1989). Experimental phase relations in the system tonalite–peridotite–H_2O at 15 Kb: implications for assimilation and differentiation processes near the crust–mantle boundary. *Journal of Petrology* **30**, 1351–1382.

Castillo, P. R., Janney, P. E. & Solidum, R. U. (1999). Petrology and geochemistry of Camiguin Island, southern Philippines: insights to the source of adakites and other lavas in a complex arc setting. *Contributions to Mineralogy and Petrology* **134**, 33–51.

Clapperton, C. M. (1993). *The Quaternary Geology and Geomorphology of South America*. Amsterdam: Elsevier, 779 pp.

Cotten, J., Le Dez, A., Bau, M., Caroff, M., Maury, R. C., Dulski, P., Fourcade, S., Bohn, M. & Brousse, R. (1995). Origin of anomalous rare-earth element and yttrium enrichments in subaerial exposed basalts: evidence from French Polynesia. *Chemical Geology* **119**, 115–138.

Dalpé, C. & Baker, D. R. (2000). Experimental investigation of large-ion-lithophile-element-, high-field-strength-element- and rare-earth-element-partitioning between calcic amphibole and basaltic melt: the effects of pressure and oxygen fugacity. *Contributions to Mineralogy and Petrology* **140**, 233–250.

Davidson, J. P., McMillan, N. J., Moorbath, S., Worner, G., Harmon, R. S. & Lopez-Escobar, L. (1990). The Nevados de Payachata volcanic region (18°S/69°W, N. Chile) II: evidence for widespread crustal involvement in Andean magmatism. *Contributions to Mineralogy and Petrology* **105**, 412–432.

Defant, M. J. & Drummond, M. S. (1990). Derivation of some modern arc magmas by melting of young subducted lithosphere. *Nature* **347**, 662–665.

Defant, M. J., Kepezhinkas, P., Wang, Q., Zhang, Q. & Xiao, L. (2001). Adakites: some variations on a theme. *Acta Petrologica Sinica* **18**, 129–142.

DePaolo, D. J. (1981). Trace element and isotopic effects of combined wallrock assimilation and fractional crystallization. *Earth and Planetary Science Letters* **53**, 189–202.

Dosso, L., Hanan, B. B., Bougault, H., Schilling, J.-G. & Joron, J.-L. (1991). Sr–Nd–Pb geochemical morphology between 10° and 17° N on the Mid-Atlantic Ridge: a new MORB isotope signature. *Earth and Planetary Science Letters* **106**, 29–43.

Drummond, M. S. & Defant, M. J. (1990). A model for trondhjemite–tonalite–dacite genesis and crustal growth via slab melting:

Archaean to modern comparisons. *Journal of Geophysical Research* **95**, 21503–21521.

Ego, F., Sébrier, M., Lavenu, A., Yepes, H. & Egüez, A. (1996). Quaternary state of stress in the Northern Andes and the restraining bend model for the Ecuadorian Andes. *Tectonophysics* **259**, 101–116.

Egüez, A., Alvarado, A., Yepes, H., Machette, M. N., Costa, C. & Dart, R. L. (2003). Database and map of Quaternary faults and folds of Ecuador and its offshore regions. Open-File Report 03–289, USGS–International Lithosphere Program Task Group II-2, Major active faults of the world.

Feininger, T. & Seguin, M. K. (1983). Simple Bouguer gravity anomaly field and the inferred crustal structure of continental Ecuador. *Geology* **11**, 40–44.

Francis, D. & Ludden, J. (1995). The signature of amphibole in mafic alkaline lavas, a study in the Northern Canadian Cordillera. *Journal of Petrology* **36**, 1171–1191.

Gaetani, G. A. & Grove, T. L. (1998). The influence of water on melting of mantle peridotite. *Contributions to Mineralogy and Petrology* **131**, 323–334.

Garcia, M. O. & Jacobson, S. S. (1979). Crystal clots, amphibole fractionation and the evolution of calc-alkaline magmas. *Contributions to Mineralogy and Petrology* **69**, 319–327.

Grove, T. L., Donnelly Nolan, J. M. & Housh, T. (1997). Magmatic processes that generated the rhyolite of Glass Mountain, Medicine Lake volcano, California. *Contributions to Mineralogy and Petrology* **127**, 205–223.

Guillier, B., Chatelain, J.-L., Jaillard, E., Yepes, H., Poupinet, G. & Fels, J.-F. (2001). Seismological evidence on the geometry of the orogenic system in central-northern Ecuador (South America). *Geophysical Research Letters* **28**, 3749–3752.

Gutscher, M.-A., Malavieille, J., Lallemand, S. & Collot, J.-Y. (1999). Tectonic segmentation of the North Andean margin: impact of the Carnegie Ridge collision. *Earth and Planetary Science Letters* **168**, 255–270.

Gutscher, M.-A., Maury, R. C., Eissen, J.-P. & Bourdon, E. (2000). Can slab melting be caused by flat subduction? *Geology* **28**, 535–538.

Halliday, A. N., Lee, D. C., Tommasin, S., Davies, G. R., Paslick, C. R., Fitton, G. J. & James, D. E. (1995). Incompatible trace elements in OIB and MORB and source enrichments in the sub oceanic mantle. *Earth and Planetary Science Letters* **133**, 379–395.

Hammersley, L. & DePaolo, D. J. (2002). Oxygen isotope evidence for the role of crustal contamination in the evolution of the Chalupas caldera system, Northern Andes, Ecuador. *EOS Transactions, American Geophysical Union* **83**(47), Fall Meeting Supplement, Abstract number V11A-1367.

Heath, E., Macdonald, R., Belkin, H. & Sigurdsson, C. H. (1998). Magmagenesis at Soufrière volcano, St. Vincent, lesser Antilles Arc. *Journal of Petrology* **39**, 1721–1764.

Kay, R. W. & Kay, S. M. (1993). Delamination and delamination magmatism. *Tectonophysics* **219**, 177–189.

Keppler, H. (1996). Constraints from partitioning experiments on the composition of subduction-zone fluids. *Nature* **380**, 237–240.

Kilian, R., Hegner, E., Fortier, S. & Satir, M. (1995). Magma evolution within the accretionary mafic basement of Quaternary Chimborazo and associated volcanoes (Western Ecuador). *Revista Geológica de Chile* **22**, 203–218.

Kretz, R. (1983). Symbols for rock-forming minerals. *American Mineralogist* **68**, 277–279.

Leake, B. E., Woolley, A. R., Arps, C. E. S., Birch, W. D., Gilbert, M. C., Grice, J. D., *et al.* (1997). Nomenclature of amphiboles: report of the Subcommittee on Amphiboles of the International Mineralogical Association, commission on new minerals and minerals' names. *American Mineralogist* **82**, 1019–1037.

Litherland, M., Aspden, J. A. & Egüez, A. (1993). Mapa Geológico de la República del Ecuador, 1/1.000.000^{e}. Quito: CODIGEM and British Geological Survey.

Litherland, M., Aspden, J. A. & Jemielita, R. A. (1994). *The Metamorphic Belts of Ecuador. British Geological Survey, Overseas Memoir* **11**, 147 pp.

Martin, H. (1986). Effect of steeper Archaean geothermal gradient on geochemistry of subduction zone magmas. *Geology* **14**, 753–756.

Martin, H. (1987). Petrogenesis of Archaean trondhjemites, tonalites, and granodiorites from eastern Finland: major and trace element geochemistry. *Journal of Petrology* **28**, 921–953.

Martin, H. (1999). Adakitic magmas: modern analogues of Archaean granitoids. *Lithos* **46**, 411–429.

Martin, H. & Moyen, J.-F. (2002). Secular changes in tonalite–trondhjemite–granodiorite composition as markers of the progressive cooling of the Earth. *Geology* **30**, 319–322.

Maury, R. C., Sajona, F. G., Pubellier, M., Bellon, H. & Defant, M. J. (1996). Fusion de la croûte océanique dans les zones de subduction/collision récentes: l'exemple de Mindanao (Philippines). *Bulletin de la Société Géologique de France* **167**, 579–595.

Monzier, M., Robin, C., Hall, M. L., Cotten, J., Mothes, P., Eissen, J.-P. & Samaniego, P. (1997). Les adakites d'Équateur: modèle préliminaire. *Comptes Rendus de l'Académie des Sciences* **324**, 545–552.

Monzier, M., Bourdon, E., Samaniego, P., Eissen, J.-P., Robin, C., Martin, H. & Cotten, J. (2003). Slab melting and Nb-enriched mantle beneath NVZ. *EUG–AGU–EGS Joint Assembly*, Nice, France, April 2003, Abstract EAE03-A-02087.

Morimoto, N., Fabries, J., Ferguson, A. K., Ginzburg, I. V., Ross, M., Seifert, F. A., *et al.* (1988). Nomenclature of pyroxenes. *Mineralogical Magazine* **52**, 535–550.

Nixon, G. T. (1988). Petrology of the younger andesites and dacites of Iztaccíhuatl Volcano, Mexico: I. Disequilibrium phenocryst assemblages as indicators of magma chamber processes. *Journal of Petrology* **29**, 213–264.

Peacock, S. M., Rushmer, T. & Thompson, A. (1994). Partial melting of subducting oceanic crust. *Earth and Planetary Science Letters* **121**, 227–244.

Pearce, J. & Parkinson, I. J. (1993). Trace element models for mantle melting: application to volcanic arc petrogenesis. In: Prichard, H. M., Alabaster, T., Harris, N. B. W. & Neary, C. R. (eds) *Magmatic Processes and Plate Tectonics. Geological Society, London, Special Publications* **76**, 373–403.

Peccerillo, P. & Taylor, S. R. (1976). Geochemistry of Eocene calc-alkaline volcanic rocks from the Kastamonu area, northern Turkey. *Contributions to Mineralogy and Petrology* **58**, 63–81.

Pennington, W. D. (1981). Subduction of the eastern Panama Basin and seismotectonics of northwestern South America. *Journal of Geophysical Research* **86**(B11), 10753–10770.

Prévot, R., Chatelain, J.-L., Guillier, B. & Yepes, H. (1996). Tomographie des Andes équatoriennes: evidence d'une continuité des Andes centrales. *Comptes Rendus de l'Académie des Sciences* **323**, 833–840.

Prouteau, G., Scaillet, B., Pichavant, M. & Maury, R. C. (1999). Fluid-present melting of ocean crust in subduction zones. *Geology* **27**, 1111–1114.

Prouteau, G., Scaillet, B., Pichavant, M. & Maury, R. C. (2001). Evidence for mantle metasomatism by hydrous silicic melts derived from subducted oceanic crust. *Nature* **410**, 197–200.

Rapp, R. P. & Watson, E. B. (1995). Dehydration melting of metabasalt at 8–32 kbar: implications for continental growth and crust–mantle recycling. *Journal of Petrology* **36**, 891–931.

Rapp, R. P., Watson, E. B. & Miller, C. F. (1991). Partial melting of amphibolite/eclogite and the origin of Archaean trondhjemites and tonalities. *Precambriam Research* **51**, 1–25.

Rapp, R. P., Shimizu, N., Norman, M. D. & Applegate, G. S. (1999). Reaction between slab-derived melts and peridotite in the mantle wedge: experimental constraints at 3·8 GPa. *Chemical Geology* **160**, 335–356.

Renne, P. R., Swisher, C. C., Deino, A. L., Karner, B. D., Owens, T. & DePaolo, D. J. (1998). Intercalibration of standards, absolute ages and uncertainties in $^{40}Ar/^{39}Ar$ dating. *Chemical Geology* **145**(1–2), 117–152.

Reynaud, C., Jaillard, E., Lapierre, H., Mamberti, M. & Mascle, G. (1999). Oceanic plateau and island arcs of southwestern Ecuador: their place in the geodynamic evolution of northwestern South America. *Tectonophysics* **307**, 235–254.

Ringwood, A. E. (1974). The petrological evolution of island arc systems. *Journal of the Geological Society, London* **130**, 235–254.

Robin, C., Hall, M. L., Jimenez, M., Monzier, M. & Escobar, P. (1997). Mojanda volcanic complex (Ecuador): development of two adjacent contemporaneous volcanoes with contrasting eruptive styles and magmatic suites. *Journal of South American Earth Sciences* **10**, 345–359.

Sajona, F. G., Maury, R. C., Bellon, H., Cotten, J., Defant, M. J. & Pubelier, M. (1993) Initiation of subduction and generation of slab melts in western and eastern Mindanao, Philippines. *Geology* **21**, 1007–1010.

Sajona, F. G., Maury, R. C., Bellon, H., Cotten, J. & Defant, M. J. (1996). High field strength element enrichment of Pliocene–Pleistocene Island arc basalts, Zamboanga Peninsula, western Mindanao (Philippines). *Journal of Petrology* **37**, 693–726.

Samaniego, P. (2001). Transition entre magmatismes calco-alcalin et adakitique dans le cas d'une subduction impliquant une ride océanique: le volcan Cayambe (Equateur). Ph.D. thesis, Université Blaise Pascal, Clermont-Ferrand, 259 pp.

Samaniego, P., Monzier, M., Robin, C. & Hall, M. L. (1998). Late Holocene eruptive activity at Nevado Cayambe Volcano, Ecuador. *Bulletin of Volcanology* **59**, 451–459.

Samaniego, P., Martin, H., Robin, C. & Monzier, M. (2002). Transition from calc-alkalic to adakitic magmatism at Cayambe volcano, Ecuador: insights into slab melts and mantle wedge interactions. *Geology* **30**, 967–970.

Schiano, P., Clocchiatti, R., Shimizu, N., Maury, R. C., Jochum, K. P. & Hofmann, A. W. (1995). Hydrous, silica-rich melts in the sub-arc mantle and their relationship with erupted arc lavas. *Nature* **377**, 595–600.

Schmidt, M. W. & Poli, S. (1998). Experimantally based water budget for dehydrating slabs and consequences for arc magma generation. *Earth and Planetary Science Letters* **163**, 361–379.

Sen, C. & Dunn, T. (1994). Dehydration melting of a basaltic composition amphibolite at 1·5 and 2·0 GPa: implications for the origin of adakites. *Contributions to Mineralogy and Petrology* **117**, 394–409.

Sen, C. & Dunn, T. (1995). Experimental modal metasomatism of a spinel lherzolite and the production of amphibole-bearing peridotite. *Contributions to Mineralogy and Petrology* **119**, 422–432.

Shaw, D. M. (1970). Trace element fractionation during anatexis. *Geochimica et Cosmochimica Acta* **34**, 237–243.

Smithies, R. H. (2000). The Archaean tonalite–trondhjemite–granodiorite (TTG) series is not an analogue of Cenozoic adakite. *Earth and Planetary Science Letters* **182**, 115–125.

Stern, C. R. & Killian, R. (1996). Role of the subducted slab, mantle wedge and continental crust in the generation of adakites from the Andean Austral Volcanic Zone. *Contributions to Mineralogy and Petrology* **123**, 263–281.

Stern, C. R., Futa, K. & Muehlenbachs, K. (1984). Isotope and trace element data for orogenic andesites from the austral Andes. In: Harmon, R. S. & Barreiro, B. A. (eds) *Andean Magmatism: Chemical and Isotopic Constraints*. Nantwich: Shiva, pp. 31–46.

Stern, R. J. (2002). Subduction zones. *Reviews of Geophysics* **40**(4), 1012, doi: 10.1029/2001RG000108.

Stern, R. J. & Ito, E. (1983). Trace-element and isotopic constraints on the source of magmas in the active volcano and Marianas island arcs, Western Pacific. *Journal of Volcanology and Geothermal Research* **18**, 461–482.

Straub, S. M. & Martin-del-Pozzo, A. L. (2001). The significance of phenocryst diversity in tephra from recent eruptions at Popocatepetl volcano (central Mexico). *Contributions to Mineralogy and Petrology* **140**, 487–510.

Sun, S.-S. & McDonough, W. F. (1989). Chemical and isotopic systematics of oceanic basalts: implications for mantle composition and process. In: Saunders, A. D. & Norry, J. M. (eds) *Magmatism in the Ocean Basins*. *Geological Society, London, Special Publications* **42**, 313–345.

Tatsumi, Y. & Eggins, S. (1995). *Subduction Zone Magmatism*. Cambridge, MA: Blackwell Science.

Tibaldi, A. & Ferrari, L. (1992). Latest Pleistocene–Holocene tectonics of the Ecuadorian Andes. *Tectonophysics* **205**, 109–125.

Ulmer, P. (1989). The dependence of the Fe^{2+}–Mg cation-partitioning between olivine and basaltic liquid on pressure, temperature and composition: an experimental study to 30 Kb. *Contributions to Mineralogy and Petrology* **101**, 261–273.

Ulmer, P. & Trommsdorff, V. (1995). Serpentine stability to mantle depths and subduction-related magmatism. *Science* **268**, 858–861.

Weber, M. B. I., Tarney, J., Kempton, P. D. & Kent, R. W. (2002). Crustal make-up of the northern Andes: evidence based on deep crustal xenolith suites, Mercaderes, SW Colombia. *Tectonophysics* **345**, 49–82.

White, W. M., McBirney, A. R. & Duncan, R. A. (1993). Petrology and geochemistry of the Galapagos islands: portrait of a pathological mantle plume. *Journal of Geophysical Research* **98**, 19533–19563.

Wilson, M. (1989). *Igneous Petrogenesis: A Global Tectonic Approach*. London: Chapman and Hall, 466 pp.

Yogodzinski, G. M. & Kelemen, P. B. (1998). Slab melting in the Aleutians: implications of an ion-probe study of clinopyroxene in primitive adakite and basalt. *Earth and Planetary Science Letters* **158**, 53–65.

Yogodzinski, G. M., Kay, R. W., Volynets, O. N., Koloskov, A. V. & Kay, S. M. (1995). Magnesian andesite in the western Aleutian Komandorsky region: implications for slab melting and process in the mantle wedge. *Geological Society of America Bulletin* **107**, 505–519.

Yogodzinski, G. M., Less, J. M., Churikova, T. G., Dorendorf, F., Wörner, G. & Volynets, O. N. (2001). Geochemical evidence for the melting of subducting oceanic lithosphere at plate edges. *Nature* **409**, 500–504.

York, D. (1969). Least-squares fitting of a straight line with correlated errors. *Earth and Planetary Science Letters* **5**, 320–324.